Stem Cell Reports
Article
ISSCR
OPEN ACCESS

Small-molecule screen reveals pathways that regulate C4 secretion in stem cell-derived astrocytes

Francesca Rapino,[1,2,3,*] Ted Natoli,[4] Francesco Limone,[1,2,3,5] Erin O'Connor,[1,2] Jack Blank,[1,2] Matthew Tegtmeyer,[1,3] William Chen,[1,2] Erika Norabuena,[1,2] Juhi Narula,[1,2] Dane Hazelbaker,[1,3] Gabriella Angelini,[1,3] Lindy Barrett,[1,3] Alison O'Neil,[1,2] Ursula K. Beattie,[1,2] Jessica M. Thanos,[6,7] Heather de Rivera,[3,8] Steven D. Sheridan,[6,7] Roy H. Perlis,[6,7] Steven A. McCarroll,[3,8] Beth Stevens,[3,9] Aravind Subramanian,[4] Ralda Nehme,[1,3] and Lee L. Rubin[1,2,3,*]

[1]Department of Stem Cell and Regenerative Biology, Harvard University, Cambridge, MA 02138, USA
[2]Harvard Stem Cell Institute, Harvard University, Cambridge, MA 02138, USA
[3]Stanley Center for Psychiatric Research, Broad Institute of MIT and Harvard, Cambridge, MA 02142, USA
[4]Broad Institute of MIT and Harvard, Cambridge, MA 02142, USA
[5]Leiden University Medical Center, LUMC, 2333 ZA Leiden, the Netherlands
[6]Center for Quantitative Health, Center for Genomic Medicine and Department of Psychiatry, Massachusetts General Hospital, Boston, MA, USA
[7]Department of Psychiatry, Harvard Medical School, Boston, MA, USA
[8]Department of Genetics, Harvard Medical School, Boston, MA, USA
[9]Department of Neurology, F.M. Kirby Neurobiology Center, Boston Children's Hospital, Harvard Medical School, Boston, MA, USA
*Correspondence: francesca_rapino@harvard.edu (F.R.), lee_rubin@harvard.edu (L.L.R.)
https://doi.org/10.1016/j.stemcr.2022.11.018

SUMMARY

In the brain, the complement system plays a crucial role in the immune response and in synaptic elimination during normal development and disease. Here, we sought to identify pathways that modulate the production of complement component 4 (C4), recently associated with an increased risk of schizophrenia. To design a disease-relevant assay, we first developed a rapid and robust 3D protocol capable of producing large numbers of astrocytes from pluripotent cells. Transcriptional profiling of these astrocytes confirmed the homogeneity of this population of dorsal fetal-like astrocytes. Using a novel ELISA-based small-molecule screen, we identified epigenetic regulators, as well as inhibitors of intracellular signaling pathways, able to modulate C4 secretion from astrocytes. We then built a connectivity map to predict and validate additional key regulatory pathways, including one involving c-Jun-kinase. This work provides a foundation for developing therapies for CNS diseases involving the complement cascade.

INTRODUCTION

The complement system is part of the first line of defense against harmful pathogens (Dunkelberger and Song, 2010). While the primary site of complement synthesis is the liver, production of complement also happens in the central nervous system (CNS) (Morgan and Gasque, 1997). In addition to its role in CNS inflammation, the complement system shapes the developing brain by controlling synaptic refinement to ensure proper brain wiring and function (Magdalon et al., 2020). In the mature human brain, aberrant activation of the complement has been observed in the CNS of patients with neurodegeneration, autoimmune diseases, and aging. Excessive complement activation gives rise to early synaptic loss, correlating with cognitive impairment in Alzheimer's disease (AD) and Tauopathy (Hong et al., 2016; Wu et al., 2019). Blocking the complement system *in vivo* rescues aberrant synaptic pruning and attenuates neuroinflammation and neurodegeneration in mouse models of AD (Dejanovic et al., 2018; Hong et al., 2016). These examples provide a strong rationale for targeting the complement system as a therapeutic approach to improving brain function.

Genetic variations in complement component 4 (C4) copy number have been linked to the increased risk of schizophrenia. In addition, schizophrenia patients exhibit elevated C4 expression in the cerebral cortex (Rey et al., 2020; Schizophrenia Working Group of the Psychiatric Genomics, 2014; Sekar et al., 2016). Although the exact mechanism underlying schizophrenia is unknown, the neuropathology of patients' brains is characterized by reduced thickness and synaptic density in the cortex (Glantz and Lewis, 2000; Thompson et al., 2001) consistent with the idea that C4 overexpression leads to enhanced microglia-mediated synaptic engulfment. (Comer et al., 2020; Yilmaz et al., 2020).

Astrocytes play a critical role in synapse formation, function, and elimination (Chaboub and Deneen, 2013). In the last decade, the contribution of astrocytes to neuropsychiatric and neurodegenerative diseases has been increasingly recognized (Druart and Le Magueresse, 2019; Seifert et al., 2006). Astrocytes and microglia are considered the immune cells of the brain due to their ability to secrete chemokines and cytokines, complement proteins, and for their phagocytic function. In particular, astrocytes express and secrete complement components, such as C1r, C1s, C2, C3, and C4, which, therefore, may act cell non-autonomously (Barnum, 1995; Gasque et al., 1995; Gordon et al.,

1992; Guttikonda et al., 2021; Lian et al., 2015). Importantly, it has been shown that astrocyte-conditioned media (ACM) can increase neuronal levels of C4 and may participate in complement-mediated synaptic pruning (Sellgren et al., 2017). Despite the importance of mouse experiments, mice and human differ. For example, mice only have one C4 gene, whereas humans have two distinct genes, C4A and C4B (Carroll et al., 1990). Recent work has begun to shed light on the connection between C4AL copy number and microglia engulfment *in vitro* and *in vivo* (Sellgren et al., 2019; Yilmaz et al., 2020).

Together, these observations suggest that identifying factors that reduce the secretion of C4 from human astrocytes might be a viable approach to lowering synaptic C4 and preserving synapses in CNS diseases. Restricted accessibility to primary human astrocyte samples limits their use for *in vitro* studies that require defined genetics and the availability of large numbers of cells, such as small-molecule or genetic screens. Human induced pluripotent stem cells (hiPSCs) offer the unique ability to generate large numbers of patient-specific differentiated cells. However, many standard protocols for differentiating astrocytes from pluripotent stem cells require an extensive culture time (up to 6 months) (Dezonne et al., 2017; Krencik et al., 2011; Palm et al., 2015; Sloan et al., 2017) and/or shorter protocols that rely on the isolation of intermediate cells, such as neural and oligodendrocyte progenitor cells (Barbar et al., 2020; Jiang et al., 2013), or repeated cell passages (Byun et al., 2020; Jovanovic et al., 2021; Leng et al., 2021; Lundin et al., 2018; Peteri et al., 2021; Santos et al., 2017; Soubannier et al., 2020; Tcw et al., 2017). To successfully develop valuable preclinical models for high-throughput screening of astrocytes, it would be preferable to have differentiation protocols that can rapidly and reproducibly generate large numbers of those cells.

To better understand the regulation of C4 in human astrocytes, we developed a new bioreactor-based protocol for the rapid, reproducible, and large-scale production of human astrocytes (hASTROs). Single-cell RNA sequencing (scRNA-seq) confirmed that this protocol produces almost exclusively cells expressing pan-astrocytic markers, albeit exhibiting different levels of maturity. Importantly, a comparison between and within cell lines confirmed the robustness and reproducibility of this differentiation method. Applying a sensitive ELISA-based method, we screened an annotated small-molecule library, identifying several pathways that modulate C4 secretion. By analyzing connectivity map (CMap) datasets, we were also able to discover additional C4 regulators. Combining these two approaches led to the discovery and validation of sets of compounds, such as chromatin remodeling inhibitors (BRD and HDAC inhibitors), NF-κB, JAK, and JNK inhibitors, among others, that reduce C4 secretion from human astrocytes. This type of platform may lead to the discovery of drugs capable of reducing levels of CNS complement potentially diminishing excessive synaptic elimination in neurodegenerative and neuropsychiatric diseases.

RESULTS

Rapid and efficient 3D differentiation of a pure population of astrocytes from pluripotent cells

To generate large numbers of human astrocytes in a short period of time, we optimized a previously published protocol (Emdad et al., 2012). In brief, the embryonic stem cell (ESC) lines HUES8 and H1 and induced pluripotent stem cell (iPSC) lines 1016A, Mito234, and Mito80, were grown as spheres in 3D spinner flasks (Rigamonti et al., 2016). Pluripotent spheres were patterned toward a neuroectodermal fate using dual SMAD inhibition and further differentiated into astrocytes utilizing a combination of neurobasal medium and cytokines. After 30 days, spheres could be dissociated and cryopreserved or expanded in astrocyte medium (Figure 1A). Bright-field images of the differentiated astrocytes (hASTROs) show that their morphology closely resembled that of primary human astrocytes (p-hASTROs) (Figures 1B and S1A). To evaluate the purity of these cultures, dissociated cells (P0) were grown until 80% confluent and assessed by flow cytometry for the astrocyte- or neuron-specific cell surface markers (CD44 and CD200) (Lundin et al., 2018; Turac et al., 2013). All cell lines tested expressed high levels of CD44 (70%–100%), with only a negligible percentage (<1%) of the cells expressing CD200 (Figures 1C and S1B). Moreover, after the first passage (P1), nearly all the cells expressed CD44 (Figures 1D and S1C). For the different lines tested, 100% of the cells expressed CD44, except for Mito234 hASTROs in which 95% of the cells expressed CD44 after the first passage (Figure 1D). Antibody labeling demonstrated that these cells expressed other canonical astrocyte markers, such as ALDH1L1, S100β, CX43, and the glutamate transporter EAAT1, at levels comparable with those of p-hASTROs. However, only a small percentage of the astrocytes differentiated using this protocol expressed the intermediate filament protein GFAP (Figures 1E, S1D, and S1E).

To evaluate the immune capability of hASTROs, supernatants were analyzed for the expression of 36 cytokines and chemokines in basal conditions or after stimulation with a TLR3 ligand (polyinosinic-polycytidylic acid [poly(I:C)]). We found that all astrocyte lines tested secreted a variety of factors, including CXCL1, MIF, and Serpin (Figures 1F and S1F). Moreover, stimulation with poly(I:C), induced secretion of pro-inflammatory cytokines and chemokines, such as IL-6, IL-8, MIP1a, and IL1RA, as described previously

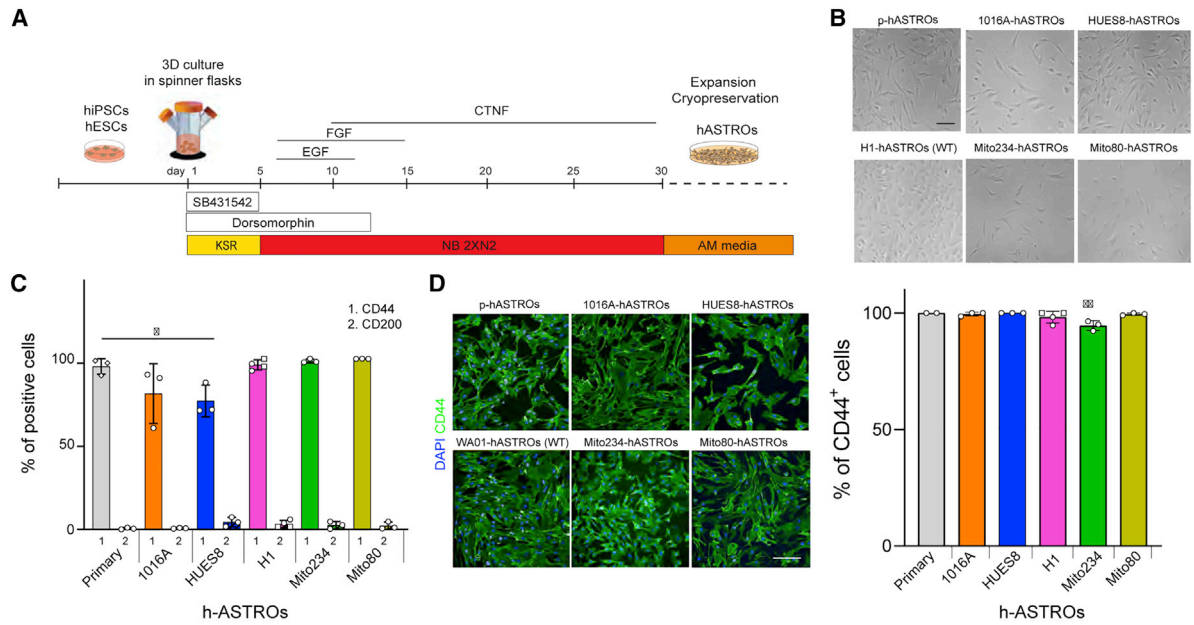

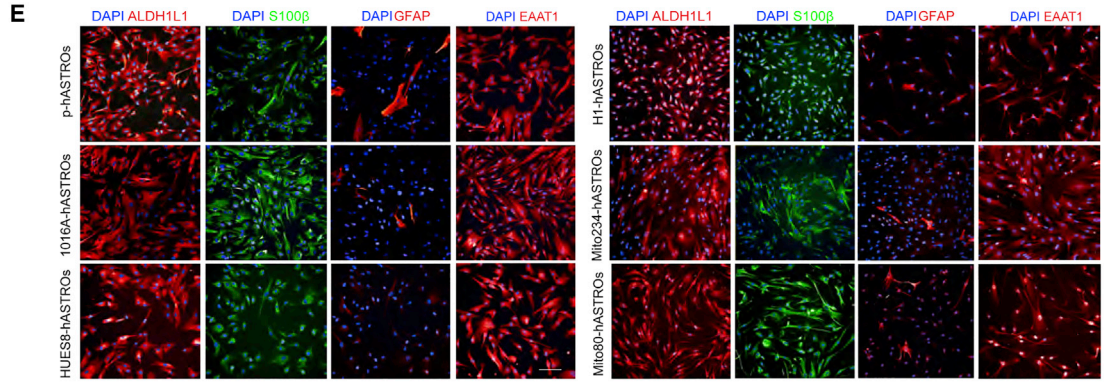

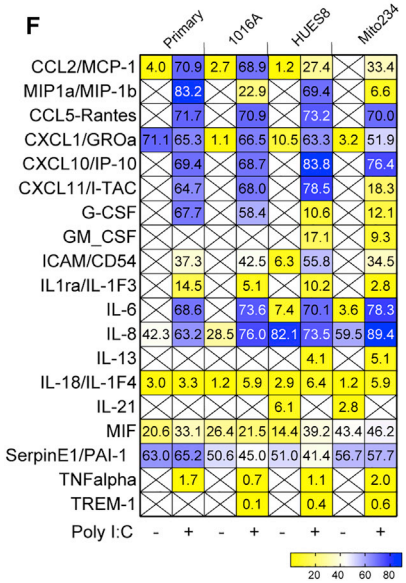

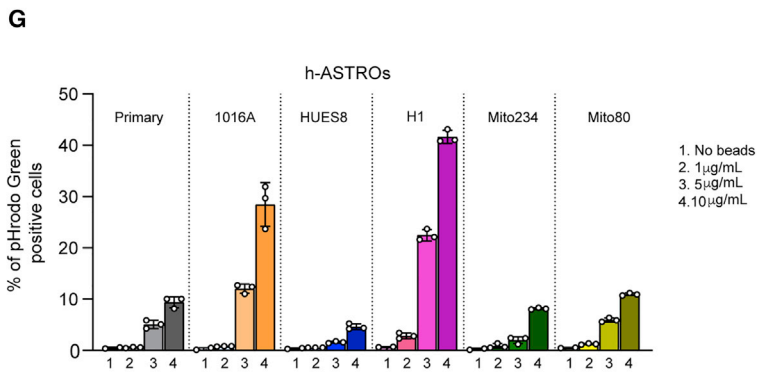

(legend on next page)

(Barbar et al., 2020; Choi et al., 2014; Tcw et al., 2017). Finally, we tested the functional phagocytic potential of hASTROs by measuring the engulfment of pHrodo green Zymosan particles (Figures 1G and S1G). We found that cell lines that were at slightly higher density when the assay was performed displayed higher percentages of GFP-positive cells (1016A and H1), suggesting that the phagocytic capacity of astrocytes may be influenced by cell density (Figure S1H).

Transcriptional profiling of stem cell-derived astrocytes

To further characterize the astrocytes to assess the reproducibility of our method, we performed scRNA-seq of three hASTRO lines (1016A, HUES8, and H1). UMAP analysis revealed equal distribution of the three lines in the populations of cells (Figure 2A). These cells expressed canonical markers of astrocytes, such as vimentin (*VIM*), *CD44*, gap junction protein alpha 1 (*GJA1*), and the *SLC1A3* gene coding for excitatory amino acid transporter 1 (EATT1) (Figure 2B). Correlation of gene expression between the different lines confirmed that there was very low inter- and intra-line variability (Figures 2C and S2A). We next evaluated the heterogeneity of these astrocytes and the potential presence of subpopulations. We were able to distinguish eight different subgroups of cells (Figure 2D). All clusters expressed pan-astrocytic markers, but none expressed oligodendrocyte or oligodendrocyte precursor (OPC) (*OLIG2*, *SOX10*, *PLP1*, and *MOG*) or neuronal markers (*DCX* and *STMN2*). We identified a group of cells (Astro2) that expressed markers of immature astrocytes or cycling cells (such as *NUSAP1*, *TOP2A*, and *CENPW*), a group of cells (Astro5) containing more progenitor-like cells (expressing *MEF2C*, *NES*, and *BCAM*), and a group (Astro4) characterized by the expression of more mature markers (*S100B*, *CD9*, and *PTPRZ1*) (Figures 2G and S2B). To determine the maturation stage of the cells, we performed hierarchical clustering of our data and compared them with available datasets of mature (adult astrocytes) and fetal primary samples (fetal cortex and fetal pre-frontal cortex [PFC GW25], as well as astrocytes and excitatory neurons [iPSC-ExN]) produced from iPSCs (Figure S2C). As expected, hASTROs clustered farther from primary adult human astrocytes, total fetal cortex, and excitatory neurons. Interestingly, iPSC-derived astrocytes clustered together and closer to PFC GW25. A further analysis of recently identified markers for mature and immature astrocytes revealed that the three cell lines analyzed expressed markers of both immature (*PPDPF*, *DTYMK*, *NUSAP1*, *TPX2*, and others) and mature astrocytes (*GLUL*, *CPE*, *NUDT3*, and others) (Figure 2H).

We assessed the regionality of hASTROs by plotting the expression of canonical dorsal and ventral markers confirming cortical identity (*RFX4*) and identifying both protoplasmic (*ID3* and *SLC14A1*) and fibrous astrocytes (*DI O 2*) (Hodge et al., 2019; Schirmer et al., 2019) (Figures 2F and S2D). Gene expression correlated with differentiation patterning, suggesting that hASTROs have a rostral, rather than caudal, anatomical localization (Figure S2D). In summary, using this 3D differentiation protocol, we can generate a homogeneous population of human astrocytes with high reproducibility between and within cell lines.

Human astrocyte secretion complement C4 is regulatable

To measure C4 secretion from hASTROs and establish a reliable screening platform, we developed an ELISA-based assay. To ensure the specificity of the antibody used, we confirmed the absence of C4 secretion from a knockout (KO) ESC line (C4 KO-hASTROs) (Figure S3A). Using this

Figure 1. Differentiation and characterization of hASTROs

(A) Schematic of hASTRO differentiation method.

(B) Representative bright-field images of primary human astrocytes (p-hASTROs) and iPSC- and ESC-hASTROs, showing astrocyte-like morphology. Scale bar, 100 μm.

(C) Flow cytometry analysis of CD44 and CD200 expression in hASTROs compared with p-hASTROs. Data are means ± SD of biological differentiations. Each symbol represents an independent differentiation (n = 3). In the H1 line, the circles represent C4 WT hASTROs (n = 2), the squares represent C4 KO hASTROs (n = 2). For primary astrocytes each symbol represents a different passage of the same batch of primary human astrocytes (n = 3). One-way ANOVA, Dunnett's multiple comparison test mean of each column versus primary human astrocytes. *Adjusted p = 0.0356.

(D) Representative immunofluorescence and quantification of CD44 expression in different cell lines. Scale bar, 100 μm. Data are means ± SD of biological differentiations (n = 3 per cell line). For H1, squares and circles represent C4 WT and C4 KO hASTROs, respectively. One-way ANOVA, Dunnett's multiple comparison test mean of each column versus primary human astrocytes. **Adjusted p = 0.0097.

(E) Representative immunocytochemistry images of astrocyte markers ALDH1L1, S100β, GFAP, and EAAT1. Blue, DAPI staining. Scale bar, 100 μm.

(F) Human cytokine array quantification of supernatants from p-hASTROs, 1016A, HUES8, and Mito234-hASTROs in basal conditions or after stimulation with poly(I:C). Heatmaps represent averages of technical duplicates.

(G) Percentage of phagocytic astrocytes (GFP-positive cells) after incubation with different concentrations of pHrodo Green Zymosan A Bioparticle conjugate.

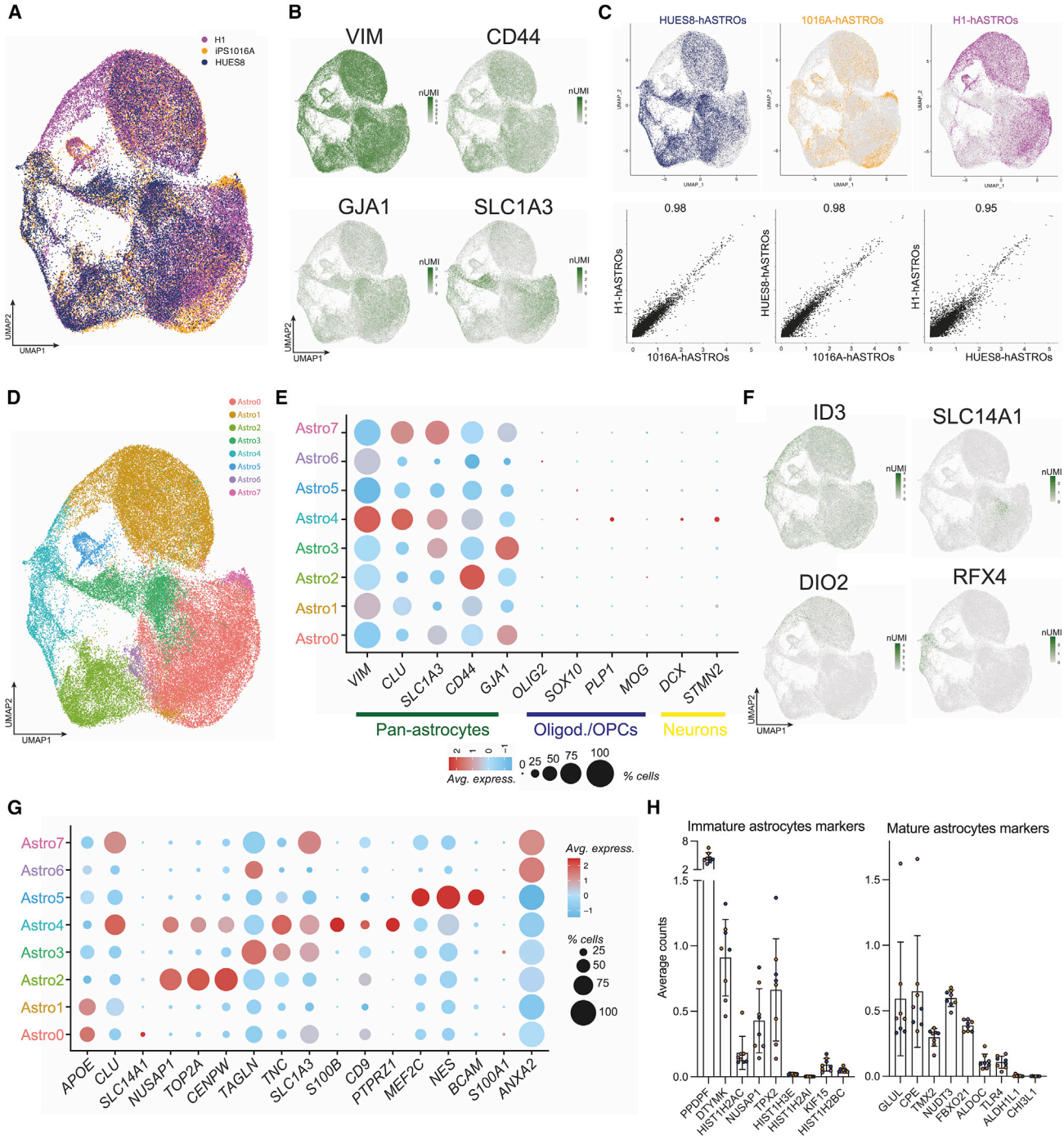

Figure 2. Transcriptomic analysis of hASTROs

(A) UMAP projection of three hASTRO lines.

(B) UMAP projections representing pan-astrocytic marker expression.

(C) UMAP projections of hASTROs from three lines with corresponding gene expression correlations.

(D) UMAP projections of identified subclusters.

(E) Dot plot for markers of different cell types in the brain.

(legend continued on next page)

assay, we found that iPSC and ESC hASTROs secreted detectable levels of C4 in basal conditions, as did pASTROs (Figures 3A and 3B). The amount of C4 secretion did not correlate with C4 copy number, since there was no significant difference observed between the lines tested (Figure 3A). C4 secretion was reduced by monensin (an ionophore that causes protein accumulation in the Golgi) and increased by treatment with interferon-γ (IFN-γ) (Walker et al., 1998) (Figure 3B).

To verify that the ELISA was only detecting human C4, we assayed the supernatant of astrocytes cultured with two different media with or without FBS. We found no differences in the amounts of C4 secreted in basal conditions or with treatment. We did observe a stronger response to IFN-γ when the cells were cultured in NB media with or without FBS (Figure S3B). To elucidate the contribution of astrocyte-derived C4 to that present at synapses, we differentiated hASTROs and Ngn2 neurons from C4-WT and KO ESCs (Figure 3C). Western blots of total lysates and concentrated ACM from hASTROs showed specific recognition of C4 bands in the WT C4-hASTRO and total absence of signal in the C4 KO-ASTROs lanes (Figures 3D and S3C). ACM collected from C4-WT or KO hASTROs was incubated with WT or KO Ngn2 neurons in different combinations, as illustrated in Figure 3C. After 24 h, synaptosomes were prepared from each of the conditions and analyzed by western blotting. As expected, no C4 bands were detected when KO ACM was incubated with KO neurons. Furthermore, no C4 was detected when WT neurons were treated with KO ACM. However, when KO neurons were incubated with WT ACM, synaptosome-bound C4 was readily detected. This indicates that, at least under these experimental conditions, C4 released from astrocytes can bind to synaptic regions and that astrocytes are the primary source of synaptic C4 protein (Figures 3D and S3C).

Small-molecule screening identifies diverse pathways able to decrease C4 secretion

To better understand the molecular mechanisms that regulate astrocyte C4 release, we used the ELISA-based assay just described, with monensin and IFN-γ as controls, to perform a small-molecule screen of 464 unique inhibitors, covering a wide variety of signaling pathways, each tested at two different concentrations. ELISAs were performed on supernatants from each well, and plates were stained with DAPI to quantify the number of nuclei per well (Figure 4A). Absorbance values were normalized for cell number; triplicates were averaged and normalized relative to DMSO controls (Figure 4B). Hits were ranked based on the percentage decrease of C4 release compared with DMSO. The top 24 compounds that were active at either one or both concentrations were selected for further analysis. An examination of the set of hit compounds confirmed that there was no bias due to the extent of representation of the compounds in the library (Figure S4A). The highest represented hit target was the bromodomain extra terminal (BET) subfamily of chromatin readers (3 compounds), followed by AKT, JAK, and p38 MAPK inhibitors (Figure 4C). Of the 24 hits, 7 compounds scored at both concentrations tested. Of those, 4 regulate gene expression and the others are inhibitors of ubiquitination, PI3K/AKT/mTOR, or JAK/STAT signaling (Figure 4D).

Selected compounds were validated using 4 different concentrations (1, 0.3, 0.1, and 0.03 μM). Of the 24 compounds tested, 20 showed a decrease of C4 in a dose-dependent manner (Figure S4B; Table S2). We then tested these compounds on hASTROs produced from an iPSC line obtained from a patient diagnosed with schizophrenia (Mito234-hASTROs). This line contains the same C4 copy number (CNV = 4) as the 1016A-hASTRO line; however, it has a different ratio of C4AL to C4BL (Figure S4C). A few compounds were somewhat more toxic to Mito234-hASTROs, as measured by a larger decrease in nuclei number after treatment (Figure S4D; Table S3). We do not yet know if this was related to the donor's disease state or to line-to-line variability. Hence, we decided to focus on compounds, including kinase inhibitors (JAK, p38 MAPK, Akt, and Src), a nuclear receptor inhibitor (PPAR antagonist), an ATPase (VCP/p97) inhibitor, and epigenetic regulators/modifiers (BET inhibitors and a BMI inhibitor), that had consistent effects on both lines.

To assess whether the difference observed in the potency of the compounds was biologically relevant, dose-response assays were conducted to identify effective concentrations for the hits in hASTROs differentiated from ESCs (HUES8 and H1) or iPSCs from healthy controls (1016A) and disease patients (Mito80 and Mito234) (Figure 4E). Log half-maximal inhibitory concentration (IC_{50}) calculation revealed that all compounds tested were effective in the nanomolar range, with BRD inhibitors (JQ1 and OTX-015) and NMS-873 on average showing higher potencies (Figure 4F). A closer look at the IC_{50} results did not reveal any correlation between the potency of the compound,

(F) UMAP projections for expression of markers associated with cortical astrocytes.
(G) Dot plots representing expression of markers characteristic of each subgroup.
(H) Expression of markers associated with astrocyte maturation. Each dot represents a biological replicate; different colors represent the different cell lines (blue HUES8, orange 1016A and purple H1).

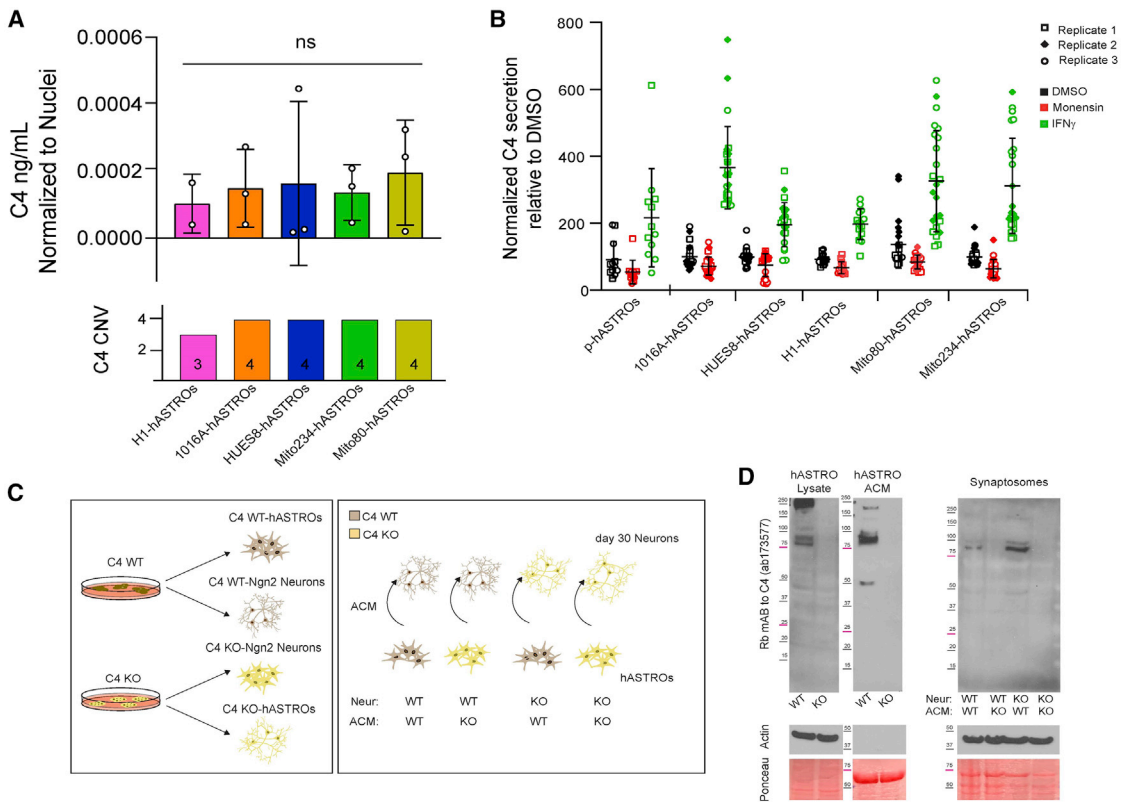

Figure 3. Human astrocytes secrete C4

(A) C4 secretion normalized to number of nuclei. Each circle represents the average of eight wells per biological replicate per line; n = 3 independent differentiations for 1016A, Hues8, Mito234, and Mito80, and n = 2 for H1. The lower panel represents the total copy number variation of C4 per line. Ordinary one-way ANOVA, Tukey's multiple comparisons test. n.s., non-significant.

(B) Normalized C4 secretion measured by ELISA comparing the effects of monensin and IFN-γ in hASTROs. Data represent individual wells (n = 8) of three biological triplicates (squares, circles, and rhombi) per line. Statistics available in Table S1.

(C) Schematic of experimental design to assess C4 detection at synaptosomes using C4 KO and C4 WT-hASTROs and Ngn2 differentiated neurons.

(D) Western blots of C4 expression in C4WT and KO-hASTROs, total lysates, and concentrated astrocyte-conditioned media (ACM) (left panel); C4 expression on synaptosomes purified from C4-WT and KO-Ngn2 neurons incubated with C4 WT or C4 KO ACM in different combinations (right panel). Ponceau and actin are used as loading controls.

the C4 copy number, and the origin of the cells (iPSC versus ESCs or heathy versus disease).

Three different pathways decrease hASTRO C4 secretion and block the response to pro-inflammatory stimuli

To explore the mechanism of C4 regulation in hASTROs, we studied the effects of compounds belonging to three different pathways: JQ1, a BET inhibitor; IMD-0354, an NF-κB inhibitor; and tofacitinib (Xeljanz), a clinically approved JAK inhibitor. These compounds are known to have anti-inflammatory properties, but their specific roles in modulating C4 secretion in human astrocytes had not been explored. We first treated 1016A and Mito234-hASTROs with JQ1 for 24 and 48 h and found a reduction in C4A and C4B mRNA at 48 h in both lines, consistent with the known effects of JQ1 on gene transcription (Figure 5A). TaqMan probes used to detect C4A and C4B were validated using the C4-KO hASTRO line (Figure S5A). To assess whether JQ1 was working as a BET inhibitor, we quantified the amount of BRD4 in the chromatin fraction of cells treated for 24 h with JQ1. We confirmed that BRD4 was displaced from chromatin, leading to a decrease in mRNA transcription (Figures 5B, S5B, and S5C). JQ1 also downregulated the mRNA levels of other key complement components, such as C1s, C2, C3, and C5 (Figure S5D).

We then asked if JQ1 could reduce the effects of two different inflammatory stimuli, IFN-γ and poly(I:C), both of which increased the secretion of C4. C4 secretion was

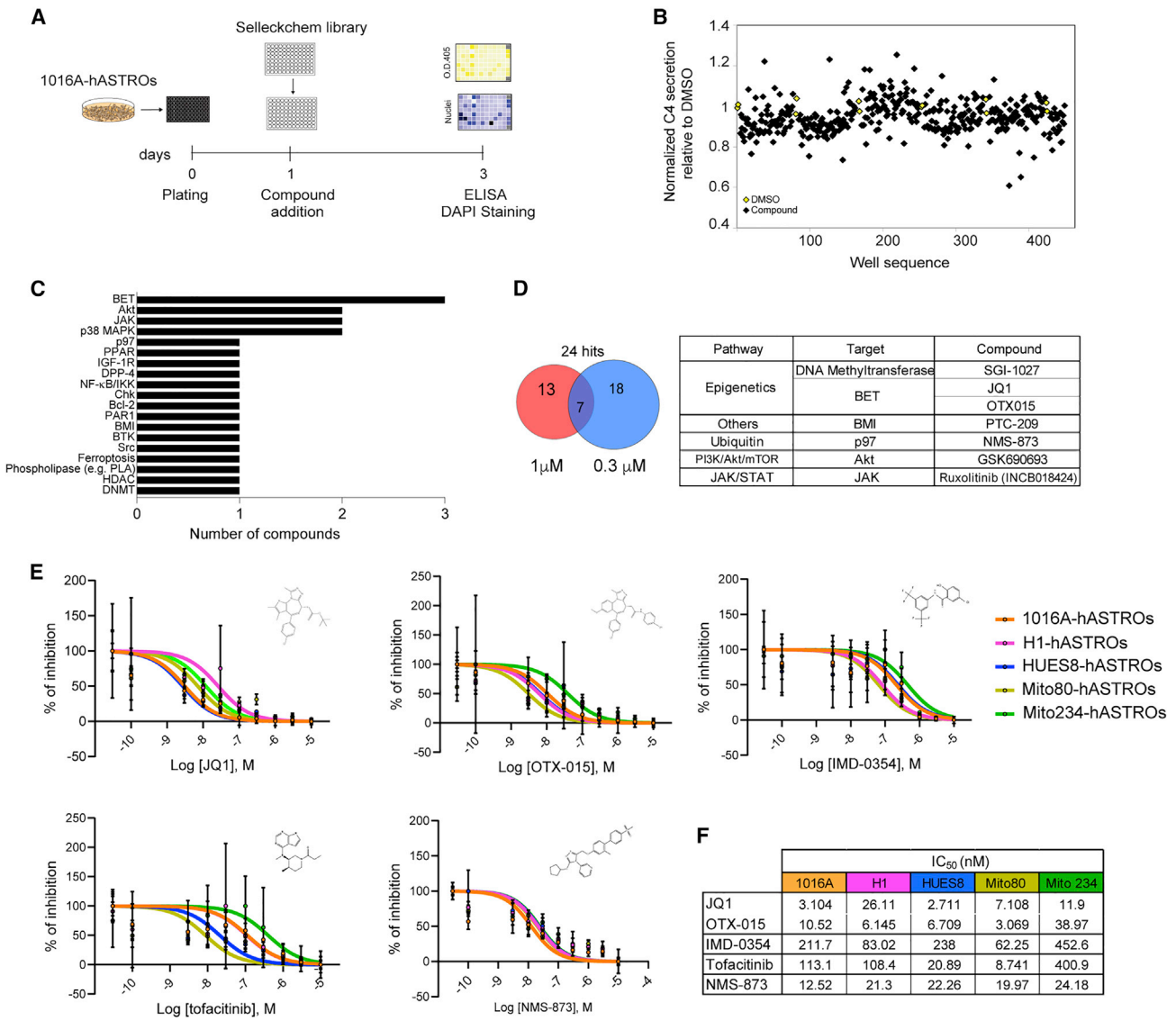

Pathway	Target	Compound
Epigenetics	DNA Methyltransferase	SGI-1027
	BET	JQ1
		OTX015
Others	BMI	PTC-209
Ubiquitin	p97	NMS-873
PI3K/Akt/mTOR	Akt	GSK690693
JAK/STAT	JAK	Ruxolitinib (INCB018424)

F

	IC_{50} (nM)				
	1016A	H1	HUES8	Mito80	Mito 234
JQ1	3.104	26.11	2.711	7.108	11.9
OTX-015	10.52	6.145	6.709	3.069	38.97
IMD-0354	211.7	83.02	238	62.25	452.6
Tofacitinib	113.1	108.4	20.89	8.741	400.9
NMS-873	12.52	21.3	22.26	19.97	24.18

Figure 4. Small-molecule screen to identify C4 modulators

(A) Schematic of the screen.

(B) Scatterplot of C4 secretion (black squares represent the average of triplicates) compared with DMSO (yellow squares are averages of triplicates) at 1 μM.

(C) Bar graph showing the targets of the identified compounds.

(D) Venn diagram showing the number of hits selected from 1 or 0.3 μM concentration and their overlap. Table shows overlapping compound targets and pathways.

(E) Normalized dose-response curves showing the percent inhibition of selected compounds tested on hASTROs. Individual points represent mean ± SD. n = 3 replicate wells for each dose; different colors represent the different cell lines tested.

(F) Table with calculated IC_{50} for JQ1, OTX-015, IMD-0354, tofacitinib, and NMS-873 in the five cell lines tested.

blocked and returned below baseline when 1016A- and Mito234-hASTROs were co-treated with pro-inflammatory stimuli and JQ1 (Figure 5C). To expand our investigation of the effects of JQ1 on cytokine secretion, we used the cytokine array already described and quantified levels of cytokines secreted from hASTROs with or without additional IFN-γ treatment. Nuclear counts were used to exclude the contribution of cell number changes (Figure S5F). Under normal culture conditions, JQ1 decreased the expression of CXCL10 and IL-8 and completely abolished the

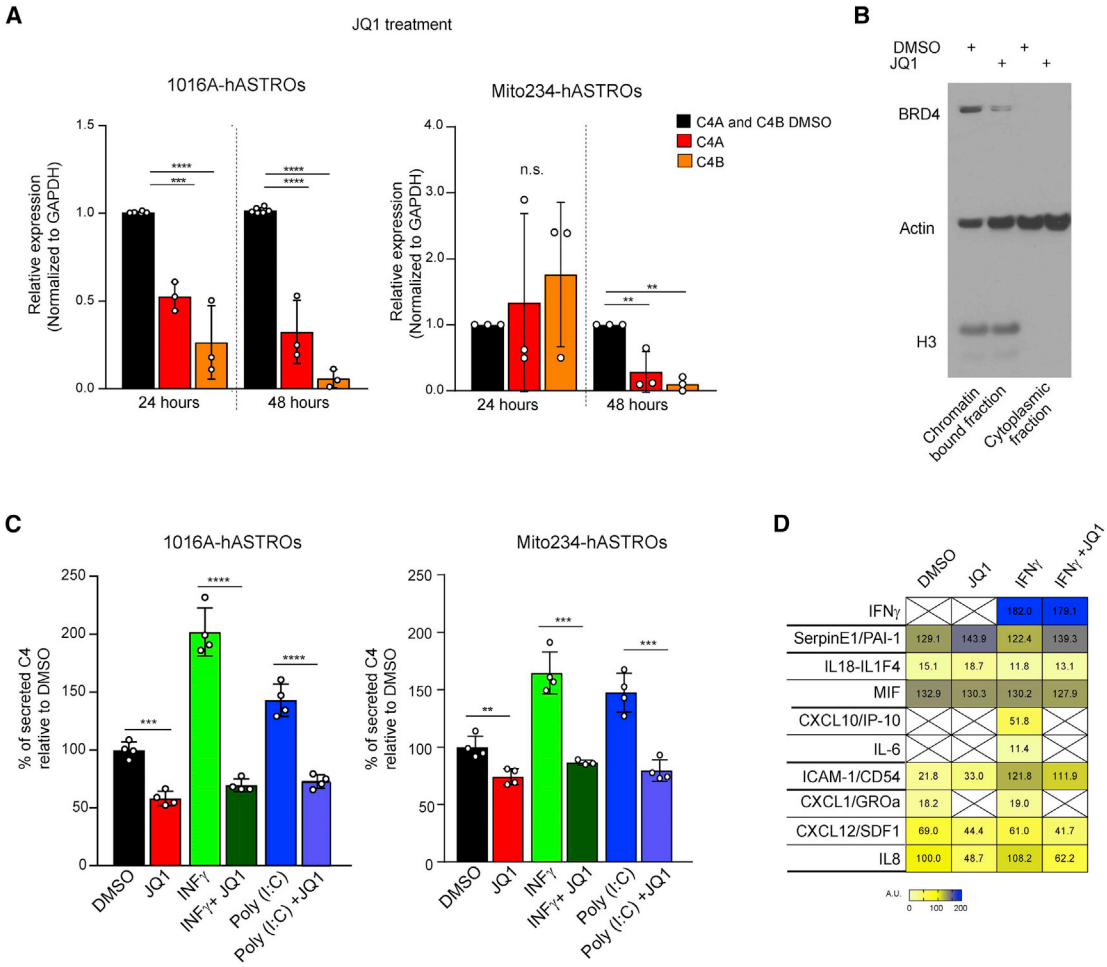

Figure 5. JQ1 represses C4 transcription and interferes with pro-inflammatory signaling

(A) qPCR of C4A and C4B in hASTROs treated with DMSO or JQ1 in 1016A and Mito234-hASTROs. Data are presented as biological triplicates. One-way ANOVA, ***p < 0.0001, ****p ≤ 0.0001, **p = 0.0026; n.s., non-significant.

(B) BRD4 displacement from chromatin in astrocytes treated with JQ1 at 1 μM for 24 h compared with DMSO control. The nuclear marker histone H3 was used as a control for the nucleus/cytoplasm fractionation.

(C) C4 ELISA of 1016A-hASTROs and Mito234-hASTROs treated with IFN-γ or poly(I:C) with or without JQ1. Data are presented as means of technical replicates ± SD relative to DMSO control (100% secretion) n = 4 wells per condition. Unpaired t test, **p = 0.005, ***p = 0.0001, ****p < 0.0001.

(D) Heatmap showing cytokine measurement in supernatants of 1016A-hASTROs treated with DMSO, IFN-γ, JQ1, or IFN-γ and JQ1.

secretion of the chemokine CXCL1. Stimulation with IFN-γ promoted the secretion of CXCL10, IL-6, and ICAM-1. JQ1 treatment entirely blocked the secretion of CXCL10 and IL-6 but had a much smaller effect on ICAM-1. No effect of JQ1 on Serpin E1, IL18, MIF, or IFN-γ secretion was observed (Figures 5D and S5E).

Next, we carried out additional studies of IMD-0354. To validate the mechanism of action (MoA) of this NF-κB inhibitor, we treated cells with poly(I:C) and measured p65 nuclear translocation (Figure S5G). As expected, quantification of the percentage of p65-positive nuclei confirmed that IMD-0345 strongly inhibits this process (Figure S5H). We next investigated the effect of IMD-0354 on C4 transcription, finding that the C4 decrease at 48 h could be mainly attributed to reducing C4B mRNA, whereas C4A was transiently upregulated after 24 h of treatment, subsequently returning to baseline levels (Figure S5I). Although similar trends were observed with Mito234-hASTROs, no statistically significant decrease of either C4A or C4B was found at 48 h. When we challenged the astrocytes with inflammatory stimuli and co-treated with IMD-0354, we observed a significant decrease in C4 secretion under all conditions tested (Figure S5J). We then looked at the effect of the JAK-STAT inhibitor tofacitinib on C4 modulation. hASTROs treated

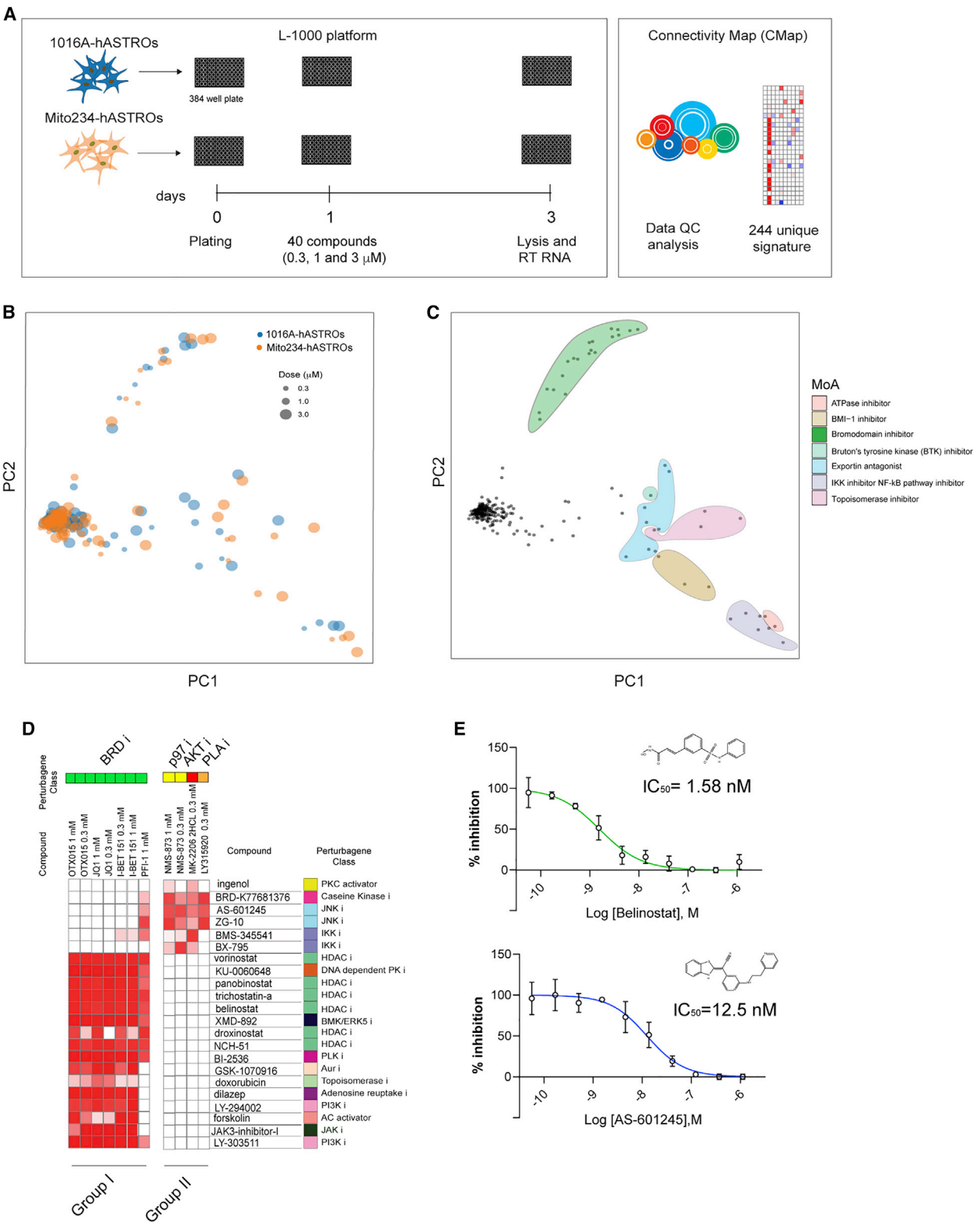

(legend on next page)

with tofacitinib showed a robust decrease in both C4A and C4B mRNA levels in 1016A- and Mito234-hASTROs (Figure S5K). Moreover, tofacitinib treatment decreased C4 secretion both under basal conditions and upon treatment with pro-inflammatory stimuli (Figure S5L).

In summary, we confirmed that three compounds targeting different signaling pathways and cellular mechanisms reduce C4 secretion from human astrocytes under baseline conditions and block the increase in secretion that was produced by treatment with two inflammatory stimuli. Interestingly, JQ1, as might have been expected, reduced the secretion of additional complement components and cytokines.

Building a CMap to predict novel C4 modulatory pathways

To broaden our ability to discover new modulatory pathways for astrocyte C4, we built a C4 CMap (C4-CMap). Drug-induced gene expression signature was generated using the high-throughput and cost-effective L1000 Luminex bead-based assay platform (Subramanian et al., 2017). In brief, L1000 measures the transcript abundance of 978 landmark genes and computational analysis can infer the expression of non-measured genes. Gene-wide robust *Z* scores are then computed across all samples in the same plate to calculate differential gene expression signatures for each sample. These signatures are used to explore relationships—similarities or dissimilarities—among diseases, drugs, genes, and pathways, by comparing their associated differential expression signatures. To generate C4-CMap data, we selected a list of perturbagens belonging to diverse pathways, such as inflammation, neuroactive compounds, chromatin remodeling, and others, based on our primary screening results. When possible, we included multiple compounds against the same target (Figure S6A). In total, we compared hASTROs and Mito234-hASTROs using 40 compounds at 3 different concentrations, generating 244 gene expression signatures (including untreated and DMSO-treated cells) (Figure 6A). Principal-component analysis of the C4-CMap signature showed no clustering bias resulting from cell origin or compound dosage (Figures 6B, S6B, and S6C). To assess what might be driving the observed separation among signatures, we used the Broad Institute's Drug Repurposing Hub (Corsello et al., 2017) to label signatures based on known MoA and targets. Closely clustered compounds are highlighted in colored groups based on the compounds' on-target mechanisms (Figure 6C). We identified seven clusters with different mechanisms of action, the largest being the bromodomain inhibitor group containing JQ1, OTX015, I-BET151, and PFI-1. Among the other identified groups, each contained one compound identified from the primary screen: IMD-0354, an IKK inhibitor; NMS-873, an ATPase inhibitor; PTC-209, a BMI inhibitor; AVL-292, a BTK inhibitor; KPT330, an Exportin-1 inhibitor; and the Topoisomerase inhibitor, mitoxantrone (used as a calibrator control for its strong and distinguishable transcriptional signature) (Figure 6C).

We then sought to leverage the CMap resource to predict other compound classes capable of affecting C4 secretion. To do this, we computed connectivity scores between the 244 C4-CMap compound signatures and the >2,400 compounds in the CMap Touchstone reference dataset. We then identified Touchstone compounds connecting preferentially to C4-CMap compounds that had previously been observed to reduce C4 secretion without decreasing cell number. This analysis revealed two groups of compounds: group I contained all the BRD inhibitors (OTX-015, JQ1, I BET, and PFI 1), and group II consisted of a p97 APTase inhibitor (NMS-873), an AKT inhibitor (MK-2206), and a PLA phospholipase inhibitor (LY315920) (Figure 6D). Connectivity results suggested that BRD inhibitors generated signatures similar to those of PLK inhibitors, PI3K inhibitors, and HDAC inhibitors. Indeed, HDAC inhibitors, such as Belinostat, were a validated hit class in our screen. The effects of Belinostat are shown in Figure 6E. The second group of compounds identified by connectivity contained multiple JNK inhibitors. Since there were no JNK inhibitors present in our original screening library, we tested an inhibitor of JNKs 1,2,3 (AS-601245) and found that it reduces C4 in a dose-dependent manner with an IC_{50} of 12.5 nM (Figure 6E).

DISCUSSION

Despite the growing interest in the role that astrocytes play in human disease, there is still a great deal to be discovered

Figure 6. Building a C4-CMap

(A) Schematic of experimental and analytic pipeline.

(B) Principal-component analysis (PCA) representing healthy control and patient cell lines treated with selected compounds. Size of circles indicates the dose of treatment.

(C) PCA projection of the two lines treated with 40 compounds at 3 doses. Clusters are colored according to the compounds' mechanisms of action (MoA).

(D) Heatmap showing the connectivity of two groups of compounds clustered by the similarity of their signatures.

(E) Dose-response curve of HDAC inhibitor (belinostat) and JNK inhibitor (AS-601245) at 72 h after treatment. Individual points represent the mean ± SD of triplicate wells.

about human glial biology. In this study, we developed a relatively rapid protocol for differentiating human pluripotent cells into astrocytes in large numbers. Compared with most existing protocols for astrocyte differentiation, our 3D method provides a straightforward and reproducible system to generate a large number of cells that can be either passaged or cryopreserved. Importantly, the cells produced by this protocol contain nearly 100% astrocytes, based on expression of canonical-astrocyte markers. Of note, this protocol is robust and reproducible when applied across pluripotent iPSC and ESC lines. Only a small percentage of differentiated cells expressed glial fibrillary acidic protein (GFAP) and primarily appear to be "resting astrocytes." As reported previously, GFAP is heterogeneously expressed in the human brain and is primarily associated with reactive states in disease (DeSilva et al., 2012; Liddelow et al., 2017; Lundin et al., 2018; Macikova et al., 2009; Tcw et al., 2017).

Crucially, astrocytes derived following this protocol secrete C4. To understand the role of C4 secretion from astrocytes and its connection to synaptic pruning, we used C4-KO lines and showed that C4 secreted from astrocytes can be a source of C4 located at synapses. This is consistent with previous data and with our scRNA-seq data on C4 expression in the mouse brain (Ximerakis et al., 2019). Although we did not detect C4 in neurons differentiated using Ngn2 overexpression, this does not exclude the possibility that other types of neurons can express and release C4. Nonetheless, these experiments suggest that decreasing secreted C4 from astrocytes can influence synaptic C4 and modulate the synaptic over-pruning observed in neuropsychiatric and neurodegenerative diseases.

Although the inhibition of complement is recognized as a potentially valuable therapeutic approach, developing useful clinical CNS complement-inhibiting drugs has been challenging, due to the limited permeability of the blood-brain barrier (BBB) (Ricklin and Lambris, 2016), although antibodies that block C1q can lessen microglia-mediated synapse loss in animal models of AD (Dejanovic et al., 2018; Hong et al., 2016). Using an ELISA-based screen we aimed to identify compounds and pathways that reduce secreted C4 from cultured human astrocytes. We focused our attention on BRD, NF-kB, and JAK inhibitors for their strong effects, and known involvement in the inflammatory response. Previous work is consistent with our observations. For example, two studies highlighted the ability of JQ1 to cross the BBB, reduce inflammation, and improve brain plasticity in both WT and mouse models of AD (Benito et al., 2017; Magistri et al., 2016). The transcription factor NF-kB is a well-known master regulator of the inflammatory response and has been implicated in neurodegenerative disease (Flood et al., 2011). Moreover, NF-κB has been shown to be activated in a mouse model of AD and to lead to increased release of C3 and subsequent effects on dendritic morphology and synaptic function (Lian et al., 2015). Finally, the JAK/STAT pathway is activated by IFN-γ, a well-known inflammatory mediator that modulates C3 and C4 levels in different cell types, including astrocytes (Kitamura et al., 1999; Mitchell et al., 1996). Our data provide evidence that JAK inhibition can prevent C4 secretion from astrocytes both under basal conditions and in response to pro-inflammatory stimuli.

To identify additional pathways that can regulate C4 in human astrocytes, we built an *in silico* CMap. As our data clearly show, CMap is a valuable and cost-effective tool to predict potentially therapeutic drug candidates in neuronal cell types, even though this dataset was generated using primarily cancer cell lines. Among the targets predicted by this analysis, HDAC inhibitors were excellent positive controls. One of the HDAC inhibitors was present in our initial hit collection and was confirmed in a secondary assay. While it might seem counterintuitive that BRD inhibitors generate a signature similar to HDAC inhibitors, it has already been shown in other cellular systems that HDAC and BRD modulate similar genes through global acetylation rearrangements, pause of RNA elongation, and selective depletion of BRD-containing proteins (Bhadury et al., 2014; Mackmull et al., 2015). Most importantly, the CMap analysis allowed us to identify and validate new targets, such as JNK, that were not covered by compounds in our screening library. Prior to this study, very little was known about the regulation of C4 in human astrocytes. Our approaches help identify multiple pathways that regulate C4 secretion and that can be targeted in different ways. One of the advantages of our study may be the possibility of repurposing drugs for serious CNS indications.

Using the CMap analysis, we also explored the transcriptional differences between hASTROs differentiated from healthy donors or patients affected by schizophrenia. We did not detect statistically meaningful differences between the lines in response to the selected perturbations. More in-depth analysis (such as RNA-seq) comparing a larger number of hASTROs lines treated with more perturbagens, may help to reveal interesting differences between healthy and disease lines.

The recent association of C4A with elevated risk of schizophrenia and its role in controlling synapse numbers motivated us to investigate the modulation of astrocyte-secreted C4 using small molecules. Understanding the mechanisms of C4 regulation and discovering C4-modulating compounds in human astrocytes is a first step toward the development of CNS penetrant complement-modulating drugs with a broad application in neuroinflammatory, neurodegenerative, and neuropsychiatric diseases. Our data provide an increased understanding of pathways that regulate C4 and that may themselves be targeted for

therapeutic application. In addition, our system permits the identification of compounds that might differentially affect C4A or C4B in human cells. The ability to distinguish between the two C4 genes might help guide the choice of the optimal C4-acting compounds.

It will come as no surprise that our hit compounds, in addition to regulating C4, modulate multiple cytokines and other complement components. The general reduction in inflammation may, therefore, synergize with the effects of decreased complement, allowing single compounds to have synergistic effects in treating serious neurodegenerative and neuropsychiatric diseases.

In conclusion, we developed a robust protocol for the differentiation of astrocytes from stem cells that can be used to interrogate human glial biology *in vitro*. We explored the biology of the regulation of C4 in human astrocytes, identifying multiple pathways that modulate its secretion. Furthermore, we built a C4-CMap that allowed us to explore and confirm new pathways able to regulate C4. The tools and knowledge that we accumulated will stimulate further research exploring C4 as a potential target for modulating synapse number and function.

EXPERIMENTAL PROCEDURES

Resource availability

Corresponding author

Further information and requests for resources and reagents should be directed to and will be fulfilled by the corresponding authors Francesca Rapino (francesca_rapino@harvard.edu or francescarapino82@gmail.com) and Lee L. Rubin (lee_rubin@harvard.edu).

Materials availability

The H1 C4 KO line generated in this study will be made available upon request, following appropriate institutional guidelines for cell line use and distribution. The 1016A and the HUES8 lines are available for request through Divvly from the HSCI iPS Core Facility. Additional cell-line-specific restrictions apply for the sharing of Mito80 and Mito234.

Data and code availability

The raw scRNA-seq data are available in NCBI's Gene Expression Omnibus (GEO) under the accession number SE213352. The processed datasets can be downloaded at https://singlecell.broadinstitute.org/single_cell/study/SCP1960/hpsc-derived-astrocytes-from-rapino-et-al-2022#study-summary. Codes used for the analysis of the RNA-seq are described in detail in supplemental experimental procedures.

hiPSC culture and astrocyte differentiation

Stem cells were cultured on Matrigel-coated plates in StemFlex medium. When PSCs reached confluency, they were dissociated to single cells using Accutase. Single suspensions of stem cells were seeded into 125 mL spinner flasks in 100 mL of mTeSR medium at a concentration of 1×10^6 cells/mL in 10 μM ROCK inhibitor Y-27632. After 48 h, the medium was changed to KSR medium with SB431542 and dorsomorphin (10 and 1 μM, respectively). The medium was changed every day for the first 5 days. From days 6 to 12, the medium was changed every 2 days with complete neurobasal supplemented with dorsomorphin, and different cytokines as specified. From day 16 onward, the medium was changed every 2 days (NB 2× N2 CTNF 20 ng/mL). At day 30, spheres were dissociated and either cryopreserved or expanded on PLL-coated plates. For details about stem cell culture, 3D astrocyte differentiation, sphere dissociation, astrocytes culture, and cryopreservation see supplemental experimental procedures.

scRNA-seq

For scRNA-seq experiments, cells were harvested and run through the 10X Chromium Single Cell 3′ Reagents V3 system according to the vendor's instructions (10X Genomics, San Francisco, CA). Samples were then sequenced on a NovaSeq 6000 system (Illumina) using an S2 flow cell at 2× 100 bp. Details about data normalization and analysis can be found in the supplemental experimental procedures.

ELISA

Ninety-six-well plates were coated with goat anti-human C4 antibody in PBS. The next day, the plates were washed and incubated with a blocking solution (1% BSA in PBS) for 1 h. After eliminating the blocking solution, astrocyte supernatant was added to each well and incubated for 1 h and 30 min. Following washes, the samples were incubated with a capture antibody to detect C4. Plates were washed three times with PBS and incubated for 30 min with goat-anti-rabbit alkaline phosphatase. In the last step, after additional washes, the plates were developed using a diethanolamine buffer. The reaction was stopped and read at 405 nm using a Molecular Devices SpectraMax M5 Reader. For antibody dilution and details on ELISA see supplemental experimental procedures and Table S4.

Screen, hit selection, secondary screen, and dose response

1016A-derived astrocytes were plated on poly-L-lysine-coated 96-well plates. The next day, the medium was replaced with fresh medium, and compounds were added at two different concentrations (1 and 0.3 μM). The screen was performed in triplicate plates using the highly selective inhibitor Library (464 compounds) from Sellckchem. Two days after compound addition, the supernatant was used to perform ELISA and plates were stained for nuclei count. Absorbance (OD_{405}) was divided by nuclei number and normalized on DMSO control (100%). Compounds were ranked by the percentage decrease of C4. The top 24 compounds were selected for a secondary validation screen. The secondary screen was performed as described previously. Cherry-picked compounds from the stock library or freshly purchased compounds were tested at four concentrations (3, 1, 0.3, and 0.1 μM) in triplicate in 1016A-hASTRO 10%. The same criteria were applied when testing compounds on Mito234-hASTROs. Twelve-point dose responses (starting at 10 μM with one to three dilutions) were performed with selected compounds in stem cell-derived astrocytes. For

details about primary screen, secondary validation, and dose-response check supplemental experimental procedures.

L1000 data generation, processing, and analysis

1016A-hASTROs and Mito234-hASTROs were plated in AM complete medium in poly-L-lysine-coated 384-well plates. The nest day, cells were treated with 40 compounds at three different concentrations in triplicate with each cell line on a separate 384-well plate. Cells were lysed after 48 h and were then subject to L1000 profiling as described in Subramanian et al. (2017). The C4-CMap signatures were converted into gene sets and queried in the CMap Touchstone (TS). C4-CMap signatures were identified as C4-reducing according to the corresponding compound's effect on C4 and lack of effect on cell fitness, using data from the C4 ELISA experiment. These signatures were then manually grouped according to the compounds' canonical MoA, resulting in two groups. We calculated the frequency with which each TS signature connected to the C4-CMap signatures in groups I and II as well as to the un-interesting C4-CMap signatures, using a threshold of $tau_{summary} \geq 90$. C4 preferential connectors were those that frequently connected to the C4-reducing signatures and infrequently to the un-interesting signatures.

SUPPLEMENTAL INFORMATION

Supplemental information can be found online at https://doi.org/10.1016/j.stemcr.2022.11.018.

AUTHOR CONTRIBUTIONS

F.R. and L.L.R. designed the project, the experiments, and wrote the manuscript. E.N. and J.N. differentiated stem cells into ASTROs, helped with the small-molecule screen, and performed follow-up experiments. A.O'N. helped perform the primary screen and U.K.B. differentiated KO-hASTROs. T.N. performed all analyses on CMap data, developed the algorithm for the analysis of C4 connectivity data, and helped write the manuscript. F.L. and M.T. performed the 10X Genomic analysis. W.C. perform the phagocytosis assay. J.B. and E.O'C. helped with cell culture and performed the FACS and the immunofluorescences, respectively. D.H., G.A., and L.B. generated the C4 KO lines. H.d.R. helped develop the ELISA protocol. J.M.T., S.D.S., R.H.P., B.S., A.S., S.A.M., and R.N. commented on the experiments and the manuscript.

ACKNOWLEDGMENTS

We thank M. Ximerakis, N. Rodriguez-Muela, J. LaLonde, F.D. Price, L. Davidow, K. Pfaff, G. Rizki, D.J. Selkoe, M. Johnson, A. Carey, J. Presumey, and Soyon Hong for helpful advice in different aspects of our work and/or for reviewing the manuscript. We also thank the staff members of the Connectivity Map (CMAP) at the Broad Institute for their technical advice and assistance. This work was supported by the Stanley Center for Psychiatric Research, the Broad Institute of Harvard and MIT, and National Institute of Mental Health grant U01MH115727 (to S.A.M. and L.L.R.), R01-MH120227 (to R.H.P., S.D.S., and J.M.T.) and P50 MH112491 (to S.A.M. and B.S.).

CONFLICT OF INTERESTS

B.S. serves on the scientific advisory board of Annexon LLC and is a minor shareholder of Annexon LLC; however, this is unrelated to the submitted work. L.L.R. is a founder of Elevian, Rejuveron, and Vesalius Therapeutics, a member of their scientific advisory boards, and a private equity shareholder. All are interested in formulating approaches intended to treat diseases of the nervous system and other tissues. He is also on the advisory board of Alkahest, a Grifols company, focused on the plasma proteome. None of these companies provided any financial support for the work in this paper. The current work is unrelated to work carried out at any of these companies. All other authors declare no competing interests.

Received: May 13, 2021
Revised: November 17, 2022
Accepted: November 19, 2022
Published: December 22, 2022

REFERENCES

Barbar, L., Jain, T., Zimmer, M., Kruglikov, I., Sadick, J.S., Wang, M., Kalpana, K., Rose, I.V.L., Burstein, S.R., Rusielewicz, T., et al. (2020). CD49f is a novel marker of functional and reactive human iPSC-derived astrocytes. Neuron *107*, 436–453.e412. https://doi.org/10.1016/j.neuron.2020.05.014.

Barnum, S.R. (1995). Complement biosynthesis in the central nervous system. Crit. Rev. Oral Biol. Med. *6*, 132–146.

Benito, E., Ramachandran, B., Schroeder, H., Schmidt, G., Urbanke, H., Burkhardt, S., Capece, V., Dean, C., and Fischer, A. (2017). The BET/BRD inhibitor JQ1 improves brain plasticity in WT and APP mice. Transl. Psychiatry *7*, e1239. https://doi.org/10.1038/tp.2017.202.

Bhadury, J., Nilsson, L.M., Muralidharan, S.V., Green, L.C., Li, Z., Gesner, E.M., Hansen, H.C., Keller, U.B., McLure, K.G., and Nilsson, J.A. (2014). BET and HDAC inhibitors induce similar genes and biological effects and synergize to kill in Myc-induced murine lymphoma. Proc. Natl. Acad. Sci. USA *111*, E2721–E2730. https://doi.org/10.1073/pnas.1406722111.

Byun, J.S., Lee, C.O., Oh, M., Cha, D., Kim, W.K., Oh, K.J., Bae, K.H., Lee, S.C., and Han, B.S. (2020). Rapid differentiation of astrocytes from human embryonic stem cells. Neurosci. Lett. *716*, 134681. https://doi.org/10.1016/j.neulet.2019.134681.

Carroll, M.C., Fathallah, D.M., Bergamaschini, L., Alicot, E.M., and Isenman, D.E. (1990). Substitution of a single amino acid (aspartic acid for histidine) converts the functional activity of human complement C4B to C4A. Proc. Natl. Acad. Sci. USA *87*, 6868–6872. https://doi.org/10.1073/pnas.87.17.6868.

Chaboub, L.S., and Deneen, B. (2013). Astrocyte form and function in the developing central nervous system. Semin. Pediatr. Neurol. *20*, 230–235. https://doi.org/10.1016/j.spen.2013.10.003.

Choi, S.S., Lee, H.J., Lim, I., Satoh, J.i., and Kim, S.U. (2014). Human astrocytes: secretome profiles of cytokines and chemokines. PLoS One *9*, e92325. https://doi.org/10.1371/journal.pone.0092325.

Comer, A.L., Jinadasa, T., Sriram, B., Phadke, R.A., Kretsge, L.N., Nguyen, T.P.H., Antognetti, G., Gilbert, J.P., Lee, J., Newmark, E.R., et al. (2020). Increased expression of schizophrenia-associated

gene C4 leads to hypoconnectivity of prefrontal cortex and reduced social interaction. PLoS Biol. *18*, e3000604. https://doi.org/10.1371/journal.pbio.3000604.

Corsello, S.M., Bittker, J.A., Liu, Z., Gould, J., McCarren, P., Hirschman, J.E., Johnston, S.E., Vrcic, A., Wong, B., Khan, M., et al. (2017). The Drug Repurposing Hub: a next-generation drug library and information resource. Nat. Med. *23*, 405–408. https://doi.org/10.1038/nm.4306.

Dejanovic, B., Huntley, M.A., De Mazière, A., Meilandt, W.J., Wu, T., Srinivasan, K., Jiang, Z., Gandham, V., Friedman, B.A., Ngu, H., et al. (2018). Changes in the synaptic proteome in Tauopathy and rescue of Tau-induced synapse loss by C1q antibodies. Neuron *100*, 1322–1336.e7. https://doi.org/10.1016/j.neuron.2018.10.014.

DeSilva, T.M., Borenstein, N.S., Volpe, J.J., Kinney, H.C., and Rosenberg, P.A. (2012). Expression of EAAT2 in neurons and protoplasmic astrocytes during human cortical development. J. Comp. Neurol. *520*, 3912–3932. https://doi.org/10.1002/cne.23130.

Dezonne, R.S., Sartore, R.C., Nascimento, J.M., Saia-Cereda, V.M., Romão, L.F., Alves-Leon, S.V., de Souza, J.M., Martins-de-Souza, D., Rehen, S.K., and Gomes, F.C.A. (2017). Derivation of functional human astrocytes from cerebral organoids. Sci. Rep. *7*, 45091. https://doi.org/10.1038/srep45091.

Druart, M., and Le Magueresse, C. (2019). Emerging roles of complement in psychiatric disorders. Front. Psychiatry *10*, 573. https://doi.org/10.3389/fpsyt.2019.00573.

Dunkelberger, J.R., and Song, W.C. (2010). Complement and its role in innate and adaptive immune responses. Cell Res. *20*, 34–50. https://doi.org/10.1038/cr.2009.139.

Emdad, L., D'Souza, S.L., Kothari, H.P., Qadeer, Z.A., and Germano, I.M. (2012). Efficient differentiation of human embryonic and induced pluripotent stem cells into functional astrocytes. Stem Cells Dev. *21*, 404–410. https://doi.org/10.1089/scd.2010.0560.

Flood, P.M., Qian, L., Peterson, L.J., Zhang, F., Shi, J.S., Gao, H.M., and Hong, J.S. (2011). Transcriptional factor NF-kappaB as a target for therapy in Parkinson's disease. Parkinsons Dis. *2011*, 216298. https://doi.org/10.4061/2011/216298.

Gasque, P., Fontaine, M., and Morgan, B.P. (1995). Complement expression in human brain. Biosynthesis of terminal pathway components and regulators in human glial cells and cell lines. J. Immunol. *154*, 4726–4733.

Glantz, L.A., and Lewis, D.A. (2000). Decreased dendritic spine density on prefrontal cortical pyramidal neurons in schizophrenia. Arch. Gen. Psychiatry *57*, 65–73.

Gordon, D.L., Avery, V.M., Adrian, D.L., and Sadlon, T.A. (1992). Detection of complement protein mRNA in human astrocytes by the polymerase chain reaction. J. Neurosci. Methods *45*, 191–197. https://doi.org/10.1016/0165-0270(92)90076-p.

Guttikonda, S.R., Sikkema, L., Tchieu, J., Saurat, N., Walsh, R.M., Harschnitz, O., Ciceri, G., Sneeboer, M., Mazutis, L., Setty, M., et al. (2021). Fully defined human pluripotent stem cell-derived microglia and tri-culture system model C3 production in Alzheimer's disease. Nat. Neurosci. *24*, 343–354. https://doi.org/10.1038/s41593-020-00796-z.

Hodge, R.D., Bakken, T.E., Miller, J.A., Smith, K.A., Barkan, E.R., Graybuck, L.T., Close, J.L., Long, B., Johansen, N., Penn, O., et al. (2019). Conserved cell types with divergent features in human versus mouse cortex. Nature *573*, 61–68. https://doi.org/10.1038/s41586-019-1506-7.

Hong, S., Beja-Glasser, V.F., Nfonoyim, B.M., Frouin, A., Li, S., Ramakrishnan, S., Merry, K.M., Shi, Q., Rosenthal, A., Barres, B.A., et al. (2016). Complement and microglia mediate early synapse loss in Alzheimer mouse models. Science *352*, 712–716. https://doi.org/10.1126/science.aad8373.

Jiang, P., Chen, C., Wang, R., Chechneva, O.V., Chung, S.H., Rao, M.S., Pleasure, D.E., Liu, Y., Zhang, Q., and Deng, W. (2013). hESC-derived Olig2+ progenitors generate a subtype of astroglia with protective effects against ischaemic brain injury. Nat. Commun. *4*, 2196. https://doi.org/10.1038/ncomms3196.

Jovanovic, V.M., Malley, C., Tristan, C.A., Ryu, S., Chu, P.-H., Barnaeva, E., Ormanoglu, P., Mercado, J.C., Michael, S., Ward, M.E., et al. (2021). Directed differentiation of human pluripotent stem cells into radial glia and astrocytes bypasses neurogenesis. Preprint at bioRxiv. https://doi.org/10.1101/2021.08.23.457423.

Kitamura, K., Andoh, A., Inoue, T., Amakata, Y., Hodohara, K., Fujiyama, Y., and Bamba, T. (1999). Sodium butyrate blocks interferon-gamma (IFN-gamma)-induced biosynthesis of MHC class III gene products (complement C4 and factor B) in human fetal intestinal epithelial cells. Clin. Exp. Immunol. *118*, 16–22. https://doi.org/10.1046/j.1365-2249.1999.01004.x.

Krencik, R., Weick, J.P., Liu, Y., Zhang, Z.J., and Zhang, S.C. (2011). Specification of transplantable astroglial subtypes from human pluripotent stem cells. Nat. Biotechnol. *29*, 528–534. https://doi.org/10.1038/nbt.1877.

Leng, K., Rose, I.V., Kim, H., Xia, W., Romero-Fernandez, W., Rooney, B., Koontz, M., Li, E., Ao, Y., Wang, S., et al. (2021). CRISPRi screens in human astrocytes elucidate regulators of distinct inflammatory reactive states. Preprint at bioRxiv. https://doi.org/10.1101/2021.08.23.457400.

Lian, H., Yang, L., Cole, A., Sun, L., Chiang, A.C.A., Fowler, S.W., Shim, D.J., Rodriguez-Rivera, J., Taglialatela, G., Jankowsky, J.L., et al. (2015). NFkappaB-activated astroglial release of complement C3 compromises neuronal morphology and function associated with Alzheimer's disease. Neuron *85*, 101–115. https://doi.org/10.1016/j.neuron.2014.11.018.

Liddelow, S.A., Guttenplan, K.A., Clarke, L.E., Bennett, F.C., Bohlen, C.J., Schirmer, L., Bennett, M.L., Münch, A.E., Chung, W.S., Peterson, T.C., et al. (2017). Neurotoxic reactive astrocytes are induced by activated microglia. Nature *541*, 481–487. https://doi.org/10.1038/nature21029.

Lundin, A., Delsing, L., Clausen, M., Ricchiuto, P., Sanchez, J., Sabirsh, A., Ding, M., Synnergren, J., Zetterberg, H., Brolén, G., et al. (2018). Human iPS-derived astroglia from a stable neural precursor state show improved functionality compared with conventional astrocytic models. Stem Cell Rep. *10*, 1030–1045. https://doi.org/10.1016/j.stemcr.2018.01.021.

Macikova, I., Perzelova, A., Mraz, P., Bizik, I., and Steno, J. (2009). GFAP-positive astrocytes are rare or absent in primary adult human brain tissue cultures. Biologia *64*, 833–839. https://doi.org/10.2478/s11756-009-0136-1.

Mackmull, M.T., Iskar, M., Parca, L., Singer, S., Bork, P., Ori, A., and Beck, M. (2015). Histone deacetylase inhibitors (HDACi) cause the selective depletion of bromodomain containing proteins (BCPs). Mol. Cell. Proteomics *14*, 1350–1360. https://doi.org/10.1074/mcp.M114.042499.

Magdalon, J., Mansur, F., Teles E Silva, A.L., de Goes, V.A., Reiner, O., and Sertié, A.L. (2020). Complement system in brain architecture and neurodevelopmental disorders. Front. Neurosci. *14*, 23. https://doi.org/10.3389/fnins.2020.00023.

Magistri, M., Velmeshev, D., Makhmutova, M., Patel, P., Sartor, G.C., Volmar, C.H., Wahlestedt, C., and Faghihi, M.A. (2016). The BET-bromodomain inhibitor JQ1 reduces inflammation and Tau phosphorylation at Ser396 in the brain of the 3xTg model of Alzheimer's disease. Curr. Alzheimer Res. *13*, 985–995. https://doi.org/10.2174/1567205013666160427101832.

Mitchell, T.J., Naughton, M., Norsworthy, P., Davies, K.A., Walport, M.J., and Morley, B.J. (1996). IFN-gamma up-regulates expression of the complement components C3 and C4 by stabilization of mRNA. J. Immunol. *156*, 4429–4434.

Morgan, B.P., and Gasque, P. (1997). Extrahepatic complement biosynthesis: where, when and why? Clin. Exp. Immunol. *107*, 1–7. https://doi.org/10.1046/j.1365-2249.1997.d01-890.x.

Palm, T., Bolognin, S., Meiser, J., Nickels, S., Träger, C., Meilenbrock, R.L., Brockhaus, J., Schreitmüller, M., Missler, M., and Schwamborn, J.C. (2015). Rapid and robust generation of long-term self-renewing human neural stem cells with the ability to generate mature astroglia. Sci. Rep. *5*, 16321. https://doi.org/10.1038/srep16321.

Peteri, U.K., Pitkonen, J., Utami, K.H., Paavola, J., Roybon, L., Pouladi, M.A., and Castrén, M.L. (2021). Generation of the human pluripotent stem-cell-derived astrocyte model with forebrain identity. Brain Sci. *11*, 209. https://doi.org/10.3390/brainsci11020209.

Rey, R., Suaud-Chagny, M.F., Bohec, A.L., Dorey, J.M., d'Amato, T., Tamouza, R., and Leboyer, M. (2020). Overexpression of complement component C4 in the dorsolateral prefrontal cortex, parietal cortex, superior temporal gyrus and associative striatum of patients with schizophrenia. Brain Behav. Immun. *90*, 216–225. https://doi.org/10.1016/j.bbi.2020.08.019.

Ricklin, D., and Lambris, J.D. (2016). New milestones ahead in complement-targeted therapy. Semin. Immunol. *28*, 208–222. https://doi.org/10.1016/j.smim.2016.06.001.

Rigamonti, A., Repetti, G.G., Sun, C., Price, F.D., Reny, D.C., Rapino, F., Weisinger, K., Benkler, C., Peterson, Q.P., Davidow, L.S., et al. (2016). Large-scale production of mature neurons from human pluripotent stem cells in a three-dimensional suspension culture system. Stem Cell Rep. *6*, 993–1008. https://doi.org/10.1016/j.stemcr.2016.05.010.

Santos, R., Vadodaria, K.C., Jaeger, B.N., Mei, A., Lefcochilos-Fogelquist, S., Mendes, A.P.D., Erikson, G., Shokhirev, M., Randolph-Moore, L., Fredlender, C., et al. (2017). Differentiation of inflammation-responsive astrocytes from glial progenitors generated from human induced pluripotent stem cells. Stem Cell Rep. *8*, 1757–1769. https://doi.org/10.1016/j.stemcr.2017.05.011.

Schirmer, L., Velmeshev, D., Holmqvist, S., Kaufmann, M., Werneburg, S., Jung, D., Vistnes, S., Stockley, J.H., Young, A., Steindel, M., et al. (2019). Neuronal vulnerability and multilineage diversity in multiple sclerosis. Nature *573*, 75–82. https://doi.org/10.1038/s41586-019-1404-z.

Schizophrenia Working Group of the Psychiatric Genomics Consortium (2014). Biological insights from 108 schizophrenia-associated genetic loci. Nature *511*, 421–427. https://doi.org/10.1038/nature13595.

Seifert, G., Schilling, K., and Steinhäuser, C. (2006). Astrocyte dysfunction in neurological disorders: a molecular perspective. Nat. Rev. Neurosci. *7*, 194–206. https://doi.org/10.1038/nrn1870.

Sekar, A., Bialas, A.R., de Rivera, H., Davis, A., Hammond, T.R., Kamitaki, N., Tooley, K., Presumey, J., Baum, M., Van Doren, V., et al. (2016). Schizophrenia risk from complex variation of complement component 4. Nature *530*, 177–183. https://doi.org/10.1038/nature16549.

Sellgren, C.M., Sheridan, S.D., Gracias, J., Xuan, D., Fu, T., and Perlis, R.H. (2017). Patient-specific models of microglia-mediated engulfment of synapses and neural progenitors. Mol. Psychiatry *22*, 170–177. https://doi.org/10.1038/mp.2016.220.

Sellgren, C.M., Gracias, J., Watmuff, B., Biag, J.D., Thanos, J.M., Whittredge, P.B., Fu, T., Worringer, K., Brown, H.E., Wang, J., et al. (2019). Increased synapse elimination by microglia in schizophrenia patient-derived models of synaptic pruning. Nat. Neurosci. *22*, 374–385. https://doi.org/10.1038/s41593-018-0334-7.

Sloan, S.A., Darmanis, S., Huber, N., Khan, T.A., Birey, F., Caneda, C., Reimer, R., Quake, S.R., Barres, B.A., and Paşca, S.P. (2017). Human astrocyte maturation captured in 3D cerebral cortical spheroids derived from pluripotent stem cells. Neuron *95*, 779–790.e6. https://doi.org/10.1016/j.neuron.2017.07.035.

Soubannier, V., Maussion, G., Chaineau, M., Sigutova, V., Rouleau, G., Durcan, T.M., and Stifani, S. (2020). Characterization of human iPSC-derived astrocytes with potential for disease modeling and drug discovery. Neurosci. Lett. *731*, 135028. https://doi.org/10.1016/j.neulet.2020.135028.

Subramanian, A., Narayan, R., Corsello, S.M., Peck, D.D., Natoli, T.E., Lu, X., Gould, J., Davis, J.F., Tubelli, A.A., Asiedu, J.K., et al. (2017). A next generation connectivity map: L1000 platform and the first 1, 000, 000 profiles. Cell *171*, 1437–1452.e17. https://doi.org/10.1016/j.cell.2017.10.049.

Tcw, J., Wang, M., Pimenova, A.A., Bowles, K.R., Hartley, B.J., Lacin, E., Machlovi, S.I., Abdelaal, R., Karch, C.M., Phatnani, H., et al. (2017). An efficient platform for astrocyte differentiation from human induced pluripotent stem cells. Stem Cell Rep. *9*, 600–614. https://doi.org/10.1016/j.stemcr.2017.06.018.

Thompson, P.M., Vidal, C., Giedd, J.N., Gochman, P., Blumenthal, J., Nicolson, R., Toga, A.W., and Rapoport, J.L. (2001). Mapping adolescent brain change reveals dynamic wave of accelerated gray matter loss in very early-onset schizophrenia. Proc. Natl. Acad. Sci. USA *98*, 11650–11655. https://doi.org/10.1073/pnas.201243998.

Turaç, G., Hindley, C.J., Thomas, R., Davis, J.A., Deleidi, M., Gasser, T., Karaöz, E., and Pruszak, J. (2013). Combined flow cytometric analysis of surface and intracellular antigens reveals surface

molecule markers of human neuropoiesis. PLoS One *8*, e68519. https://doi.org/10.1371/journal.pone.0068519.

Walker, D.G., Kim, S.U., and McGeer, P.L. (1998). Expression of complement C4 and C9 genes by human astrocytes. Brain Res. *809*, 31–38.

Wu, T., Dejanovic, B., Gandham, V.D., Gogineni, A., Edmonds, R., Schauer, S., Srinivasan, K., Huntley, M.A., Wang, Y., Wang, T.M., et al. (2019). Complement C3 is activated in human AD brain and is required for neurodegeneration in mouse models of amyloidosis and Tauopathy. Cell Rep. *28*, 2111–2123.e6. https://doi.org/10.1016/j.celrep.2019.07.060.

Ximerakis, M., Lipnick, S.L., Innes, B.T., Simmons, S.K., Adiconis, X., Dionne, D., Mayweather, B.A., Nguyen, L., Niziolek, Z., Ozek, C., et al. (2019). Single-cell transcriptomic profiling of the aging mouse brain. Nat. Neurosci. *22*, 1696–1708. https://doi.org/10.1038/s41593-019-0491-3.

Yilmaz, M., Yalcin, E., Presumey, J., Aw, E., Ma, M., Whelan, C.W., Stevens, B., McCarroll, S.A., and Carroll, M.C. (2020). Overexpression of schizophrenia susceptibility factor human complement C4A promotes excessive synaptic loss and behavioral changes in mice. Nat. Neurosci. *24*, 214–224. https://doi.org/10.1038/s41593-020-00763-8.

Stem Cell Reports, Volume *18*

Supplemental Information

Small-molecule screen reveals pathways that regulate C4 secretion in stem cell-derived astrocytes

Francesca Rapino, Ted Natoli, Francesco Limone, Erin O'Connor, Jack Blank, Matthew Tegtmeyer, William Chen, Erika Norabuena, Juhi Narula, Dane Hazelbaker, Gabriella Angelini, Lindy Barrett, Alison O'Neil, Ursula K. Beattie, Jessica M. Thanos, Heather de Rivera, Steven D. Sheridan, Roy H. Perlis, Steven A. McCarroll, Beth Stevens, Aravind Subramanian, Ralda Nehme, and Lee L. Rubin

Supplementary information

Figure S1

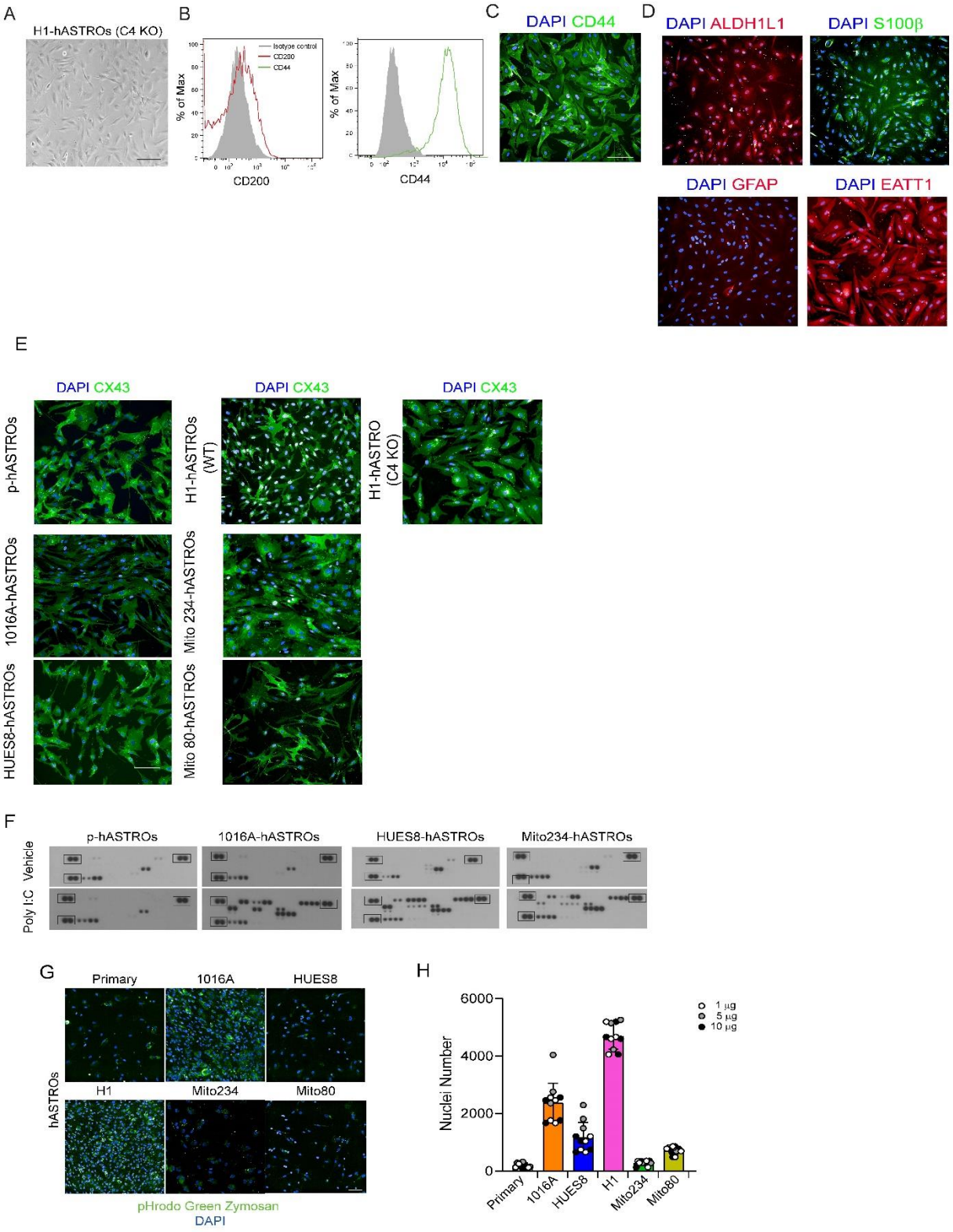

Figure S1. Related to Figure 1. **Differentiation and characterization of stem cell-derived astrocytes compared to primary human fetal astrocytes (p-hASTROs).**

(A) Bright-field image of H1 C4 KO hASTROs. (Scale bar, 100 μm). (B) Flow-cytometer analysis of astrocytes stained for neuronal marker CD200 (red), astrocyte-specific antigen CD44 (green), and relative isotype controls (grey). (C) Immunocytochemistry of CD44 in H1 C4 KO hASTROs. (D) Representative immunocytochemistry using antibodies against ALDH1L1, S100β, GFAP and EATT1 in H1 C4 KO hASTROs. (E) Immunocytochemistry of CX43 in p-ASTROs and iPSCs and ESCs derived-hASTROs. (F) Dot blot of cytokine arrays in Fig. 1F. (G) Representative images of pHrodo Green Zymosan beads after engulfment in p-ASTROs, iPSCs- and ESCs- derived hASTROs. (H) Nuclei number of replicate wells for data shown in Figure 1G. n=9 field per well acquired. Each symbol represents the sum of nuclei number per well. Each color represents a different treatment (1, 5 or 10 μg) of pHrodo Green Zymosan particles.

Figure S2

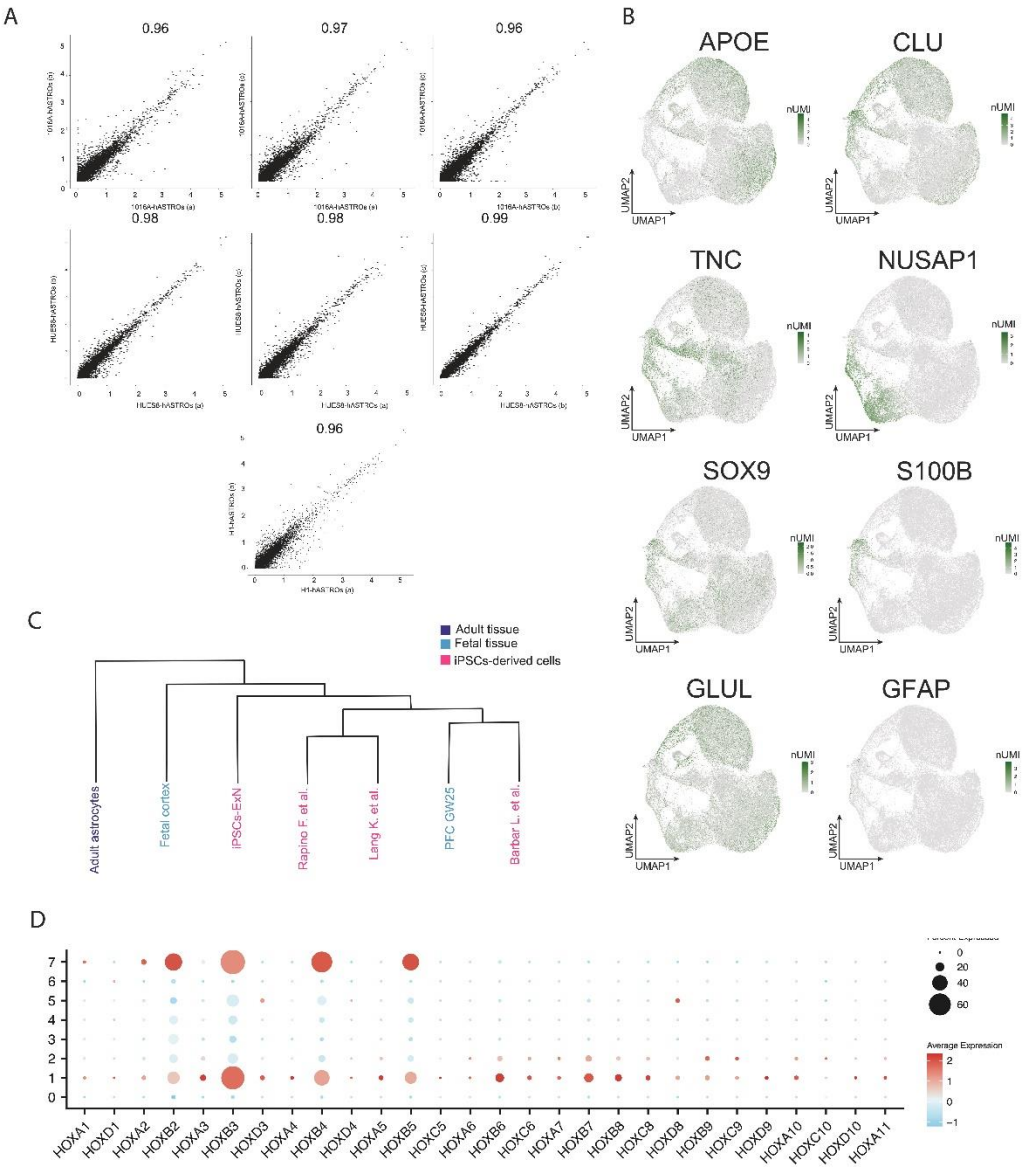

Figure S2. Related to Figure 2. **Transcriptional analysis of h-ASTROs: robustness of the differentiation protocol and regionality of the differentiated population.**
(A) Gene expression correlation between each cell line and each replicate per line. (B) UMAP projection representing markers associated with astrocyte maturation. (C) Hierarchical clustering of hASTROs and primary human astrocytes, fetal cortex and iPSC-derived astrocytes using different differentiation methods. (D) Dot plot for gene expression of all HOX genes detected in 8 astrocyte subgroups.

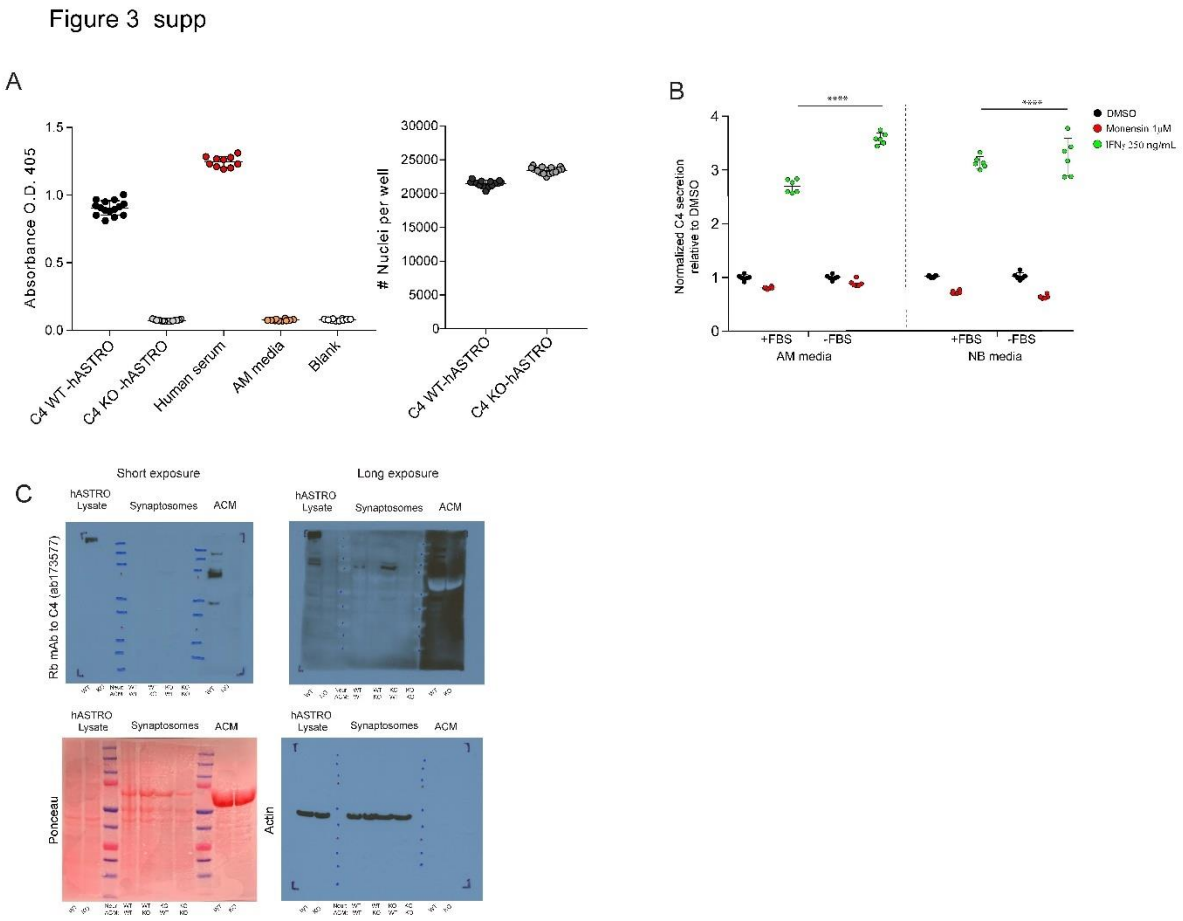

Figure S3. Related to Figure 3. **Validation of C4 secretion in different media conditions and using H1 C4 KO.**

(A) ELISA performed using C4 KO-hASTROs compared to C4 WT-hASTROs. Human serum (containing complement) was used as a positive control. Astrocyte Medium (AM) was used as a negative control. The right panel shows the number of nuclei in wells quantified in the ELISA. (B) C4 secretion in 1016A-hASTROs, cultured in different media with or without fetal bovine serum (FBS) and treated with monensin and IFNγ. AM=Astrocyte medium; NB=Neurobasal medium. Data are represented as mean of technical replicate wells (n=6, per condition) ± SD Two-way ANOVA ****p>0.0001. (C) Unprocessed Western blot films and membranes from Fig. 2D stained with C4, Ponceau and Actin.

Figure S4

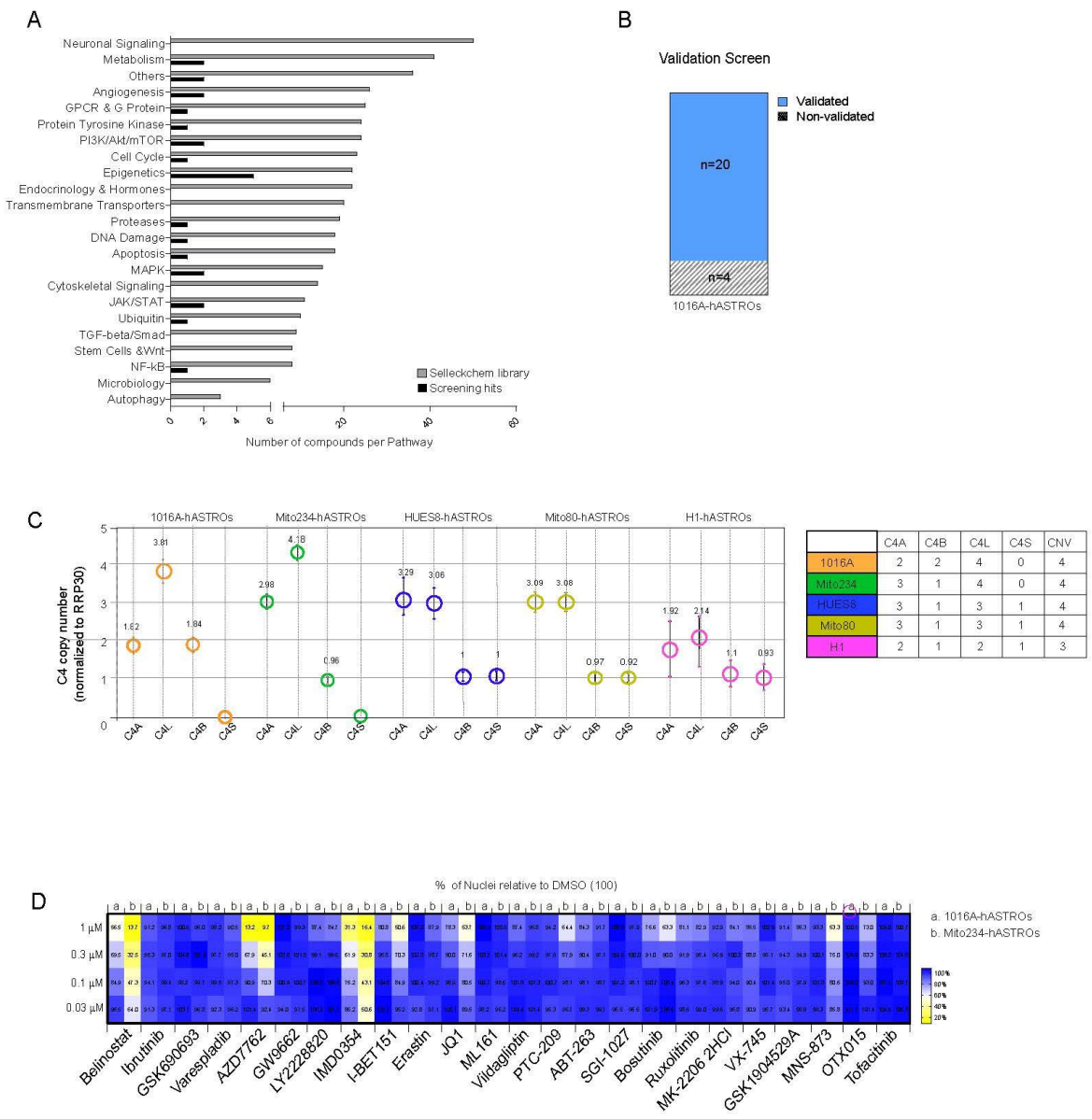

	C4A	C4B	C4L	C4S	CNV
1016A	2	2	4	0	4
Mito234	3	1	4	0	4
HUES8	3	1	3	1	4
Mito80	3	1	3	1	4
H1	2	1	2	1	3

Figure S4. Related to Figure 5. **Primary screening analysis and secondary screening validation.** (A) The bar graph shows the selected screening hits (black bars) and the content of the compounds in the Selleck Chemicals library organized by annotated pathways (grey bars). (B) Summary of validated hits in secondary screening performed on 1016A-hASTROs. Graph shows the number of validated and non-validated compounds. (C) Chart showing the total copy number and the different forms of C4 (C4A, C4B, C4L, and C4S) in 5 stem cell lines used for astrocyte differentiation. Right panel summarizes the total copy number variation of C4. (D) Nuclei number of the 1016A- and Mito234-hASTROs treated with 24 selected compounds at different concentrations, compared to DMSO treated cells (set at 100%).

Figure S5

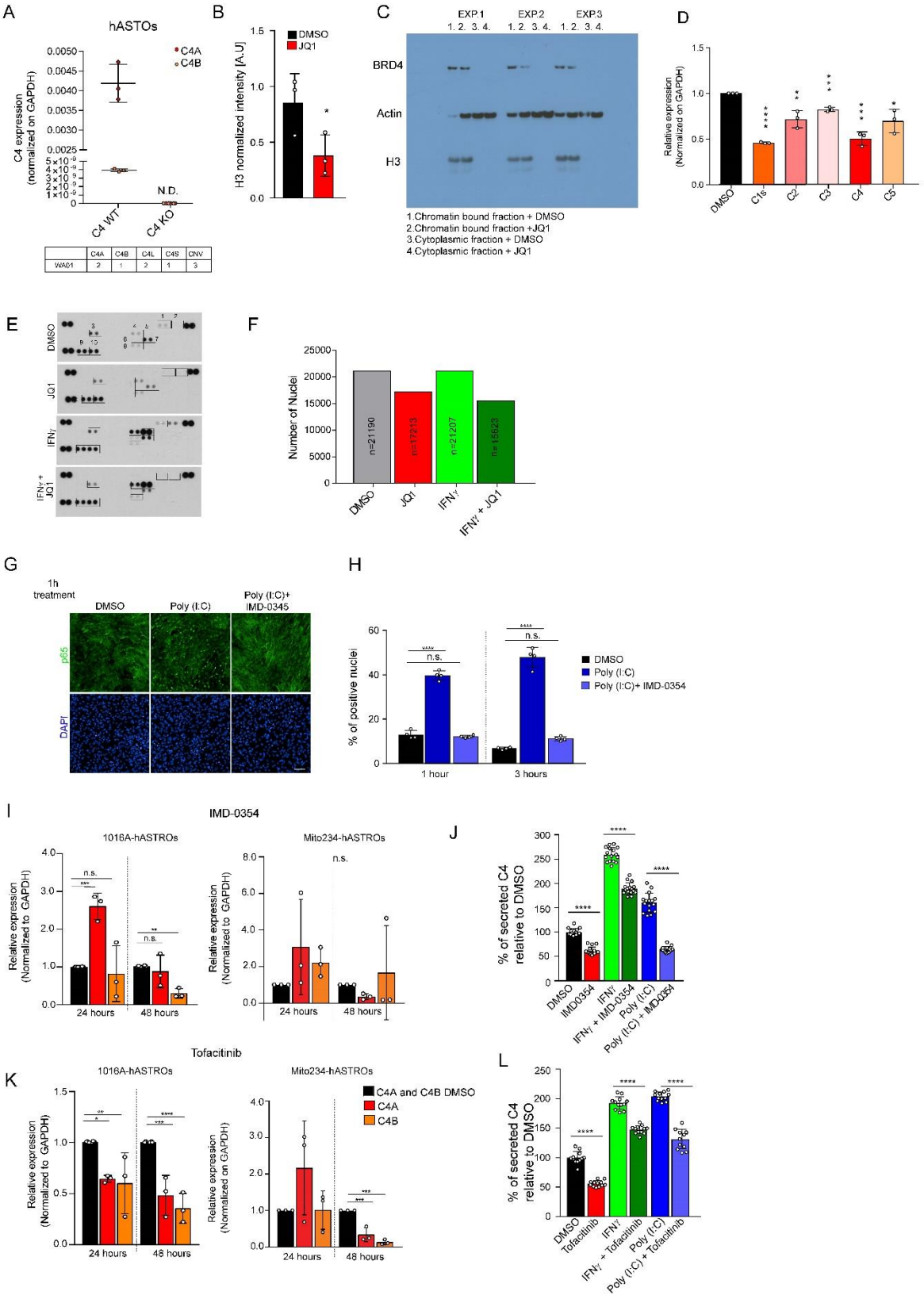
A
hASTOs
C4A
C4B
C4 expression (normalized on GAPDH)
N.D.
C4 WT
C4 KO
C4A C4B C4L C4S CNV
WA01 2 1 2 1 3
B
DMSO
JQ1
H3 normalized intensity [A.U]
C
EXP.1 EXP.2 EXP.3
1. 2. 3. 4. 1. 2. 3. 4. 1. 2. 3. 4.
BRD4
Actin
H3
1.Chromatin bound fraction + DMSO
2.Chromatin bound fraction +JQ1
3.Cytoplasmic fraction + DMSO
4.Cytoplasmic fraction + JQ1
D
Relative expression (Normalized on GAPDH)
DMSO C1s C2 C3 C4 C5
E
DMSO
JQ1
IFNγ
IFNγ + JQ1
F
Number of Nuclei
n=21190
n=17213
n=21207
n=15823
DMSO JQ1 IFNγ IFNγ + JQ1
G
1h treatment
DMSO
Poly (I:C)
Poly (I:C)+ IMD-0345
p65
DAPI
H
% of positive nuclei
n.s.
1 hour
3 hours
DMSO
Poly (I:C)
Poly (I:C)+ IMD-0354
I
IMD-0354
1016A-hASTROs
Mito234-hASTROs
Relative expression (Normalized to GAPDH)
24 hours
48 hours
J
% of secreted C4 relative to DMSO
DMSO
IMD0354
IFNγ
IFNγ + IMD-0354
Poly (I:C)
Poly (I:C) + IMD0354
Tofacitinib
K
1016A-hASTROs
Mito234-hASTROs
C4A and C4B DMSO
C4A
C4B
L
% of secreted C4 relative to DMSO
DMSO
Tofacitinib
IFNγ
IFNγ + Tofacitinib
Poly (I:C)
Poly (I:C) + Tofacitinib

Figure S5. Related to Figure 5. **Effects of JQ1, IMD-0354, and Tofacitinib on C4 mRNA and secretion.**

(A) Specificity of TaqMan probes for C4A and C4B assessed using the C4 KO-hASTRO line. The table below shows the copy number variation of C4 in the H1 cell line used to generate the KO. (B) Bar graph quantifies BRD4 on the chromatin fraction after treatment of biological triplicates with DMSO or JQ1. Unpaired t-test, *p< 0.01. (C) Unprocessed Western blot film of Fig. 3B. Western blot was run on triplicate experiments (EXP1, EXP2 and EXP3) and stained for BDR4, Actin and H3 to label the chromatin and cytoplasmic fractions. (D) qPCR expression of different complement components (including total C4) in biological triplicates of 1016A-hASTROs treated with JQ1. Unpaired t-test, *p< 0.01, **p≤ 0.001, ***p< 0.0001, ****p≤ 0.0001. (E) Dot blots of human cytokine profile quantified in Fig. 3D. Unlabeled dots are positive technical controls. Numbered rectangles represent different cytokines quantified. (F) Total nuclei number of astrocytes used for the detection of cytokines in Fig. 5D. (G) Representative images of NF-κB p65 immunostaining in astrocytes treated with poly(I:C) alone or in combination with IMD-0354. Scale bar 100 μM. (H) Quantification of the percent of p65-positive nuclei after one or three hours of treatment in technical replicates. One-way ANOVA, comparing treatment to DMSO ****p≤ 0.0001. (I) C4A and C4B mRNA expression of biological triplicates of 1016A and Mito234-hASTROs treated with IMD-0354 for 24 or 48 hours. One-way ANOVA, **p≤ 0.001, ***p< 0.0001, n.s.=non-significant. (J) ELISA of secreted C4 in 1016A-hASTROs treated with the NF-κB inhibitor with or without IFNγ or poly(I:C). Data are presented as mean of technical replicates ± SD relative to DMSO control (100% secretion). Unpaired t-test ****p< 0.0001. (K) C4A and C4B mRNA expression of biological triplicates of 1016A and Mito234-hASTROs treated with Tofacitinib for 24 or 48 hours. One-way ANOVA, *p< 0.01, **p≤ 0.001, ***p< 0.0001, ****p≤ 0.0001, n.s.=non-significant. (L) ELISA of secreted C4 in 1016A-hASTROs treated with Tofacitinib with or without IFNγ or poly(I:C). Data are presented as mean of technical replicates ± SD relative to DMSO control (100% secretion). Unpaired t-test ****p< 0.0001.

Figure S6

A

Compounds	Target
(+)- JQ1	BRD
OTX-015	
PFI-1	
I-BET151	
Ruxolitinib	JAK
Tofacitinib	
LY2784544	
Pacritinib	
Ilgotinib	
NMS-873	p97
IMD-0354	IkB/IKK
Vildagliptin	DPP-4
Trelagliptin	
Erastin	Ferroptosis
Ferrostatin-1	
MK-2206 2HCl	AKT
GSK690693	
GDC-0068	
GW9662	PPAR
T0070907	
Ibrutinib	BTK
CGI1746	
AVL-292	
CNX-774	
LY315920	PLA phospholipase
PTC-209	BMI
ML161	PAR1
FTY720	S1RP
SKI II	
SB742457	5-HT Receptor
Tolazoline HCl	Adrenergic receptor
Aniracetam	AMPA Receptor
EUK 134	Beta Amyloid
Naproxen	COX
KPT-330	CRM1
Clemastine Fumate	Histamine receptor
Batimastat	MMP
Allopurinol	OX receptor
SU11274	c-Met

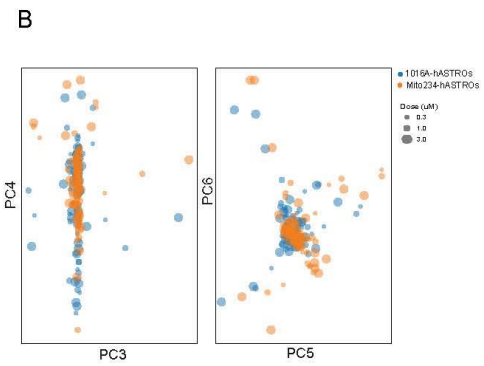

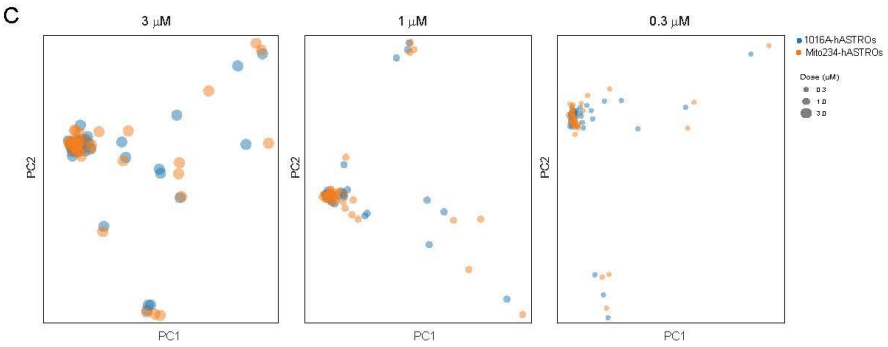

Figure S6. Related to Figure 6. **C4 connectivity through CMap analysis**.
(A) Table of selected compounds used for the CMap analysis. (B) PC3 vs. PC4 and PC5 vs. PC6 of healthy control (1016A-pASTROs) and patient cell line (Mito234-hASTROs) treated with selected compounds. Circles of different sizes represent different doses (0.3, 1, and 3 μM). (C) PCA (PC 1 vs. PC2) of the two cell lines plotted per dose. PCA was performed on the data from each dose independently.

Table S1
Statistics of Figure 3B

Tukey's multiple comparisons test	Mean Diff.	95.00% CI of diff.	Below threshold?	Summary	Adjusted P Value
H1 hASTROs DMSO vs. H1 hASTROs Monensin	25.42	-75.46 to 126.3	No	ns	>0.9999
H1 hASTROs DMSO vs. H1 hASTROs IFNy	-105.3	-206.2 to -4.405	Yes	*	0.0304
H1 hASTROs DMSO vs. Primary HA DMSO	1.181	-103.8 to 106.2	No	ns	>0.9999
H1 hASTROs DMSO vs. Primary HA Monensin	38.18	-69.36 to 145.7	No	ns	0.9988
H1 hASTROs DMSO vs. Primary HA IFNy	-124	-229.0 to -18.95	Yes	**	0.0053
H1 hASTROs DMSO vs. Mito80 hASTROs DMSO	-43.71	-133.5 to 46.05	No	ns	0.9633
H1 hASTROs DMSO vs. Mito80 hASTROs Monensin	8.186	-81.58 to 97.95	No	ns	>0.9999
H1 hASTROs DMSO vs. Mito80 hASTROs IFNy	-233.7	-323.5 to -143.9	Yes	****	<0.0001
H1 hASTROs DMSO vs. Mito234 hASTROs DMSO	-7.515	-97.28 to 82.25	No	ns	>0.9999
H1 hASTROs DMSO vs. Mito 234 hASTROs Monensin	28.23	-62.25 to 118.7	No	ns	0.9998
H1 hASTROs DMSO vs. Mito 234 hASTROs IFNy	-219.6	-309.3 to -129.8	Yes	****	<0.0001
H1 hASTROs DMSO vs. Hues8 hASTROs DMSO	-7.23	-96.99 to 82.53	No	ns	>0.9999
H1 hASTROs DMSO vs. Hues8 hASTROs Monensin	17.35	-72.41 to 107.1	No	ns	>0.9999
H1 hASTROs DMSO vs. Hues8 hASTROs IFNy	-103	-192.7 to -13.19	Yes	**	0.0084
H1 hASTROs DMSO vs. 1016A hASTROs DMSO	-7.515	-97.28 to 82.25	No	ns	>0.9999
H1 hASTROs DMSO vs. 1016A hASTROs Monensin	20.65	-69.12 to 110.4	No	ns	>0.9999
H1 hASTROs DMSO vs. 1016A hASTROs IFNy	-273.7	-363.5 to -184.0	Yes	****	<0.0001
H1 hASTROs Monensin vs. H1 hASTROs IFNy	-130.7	-231.6 to -29.83	Yes	***	0.001
H1 hASTROs Monensin vs. Primary HA DMSO	-24.24	-129.2 to 80.76	No	ns	>0.9999
H1 hASTROs Monensin vs. Primary HA Monensin	12.75	-94.79 to 120.3	No	ns	>0.9999
H1 hASTROs Monensin vs. Primary HA IFNy	-149.4	-254.4 to -44.37	Yes	***	0.0001
H1 hASTROs Monensin vs. Mito80 hASTROs DMSO	-69.13	-158.9 to 20.63	No	ns	0.3792
H1 hASTROs Monensin vs. Mito80 hASTROs Monensin	-17.24	-107.0 to 72.52	No	ns	>0.9999

H1 hASTROs Monensin vs. Mito80 hASTROs IFNy	-259.1	-348.9 to -169.4	Yes	****	<0.0001
H1 hASTROs Monensin vs. Mito234 hASTROs DMSO	-32.94	-122.7 to 56.82	No	ns	0.9983
H1 hASTROs Monensin vs. Mito 234 hASTROs Monensin	2.807	-87.67 to 93.28	No	ns	>0.9999
H1 hASTROs Monensin vs. Mito 234 hASTROs IFNy	-245	-334.8 to -155.2	Yes	****	<0.0001
H1 hASTROs Monensin vs. Hues8 hASTROs DMSO	-32.65	-122.4 to 57.11	No	ns	0.9984
H1 hASTROs Monensin vs. Hues8 hASTROs Monensin	-8.073	-97.83 to 81.69	No	ns	>0.9999
H1 hASTROs Monensin vs. Hues8 hASTROs IFNy	-128.4	-218.1 to -38.61	Yes	***	0.0001
H1 hASTROs Monensin vs. 1016A hASTROs DMSO	-32.94	-122.7 to 56.82	No	ns	0.9983
H1 hASTROs Monensin vs. 1016A hASTROs Monensin	-4.777	-94.54 to 84.98	No	ns	>0.9999
H1 hASTROs Monensin vs. 1016A hASTROs IFNy	-299.2	-388.9 to -209.4	Yes	****	<0.0001
H1 hASTROs IFNy vs. Primary HA DMSO	106.5	1.466 to 211.5	Yes	*	0.0428
H1 hASTROs IFNy vs. Primary HA Monensin	143.5	35.92 to 251.0	Yes	***	0.0006
H1 hASTROs IFNy vs. Primary HA IFNy	-18.66	-123.7 to 86.34	No	ns	>0.9999
H1 hASTROs IFNy vs. Mito80 hASTROs DMSO	61.58	-28.18 to 151.3	No	ns	0.5995
H1 hASTROs IFNy vs. Mito80 hASTROs Monensin	113.5	23.71 to 203.2	Yes	**	0.0016
H1 hASTROs IFNy vs. Mito80 hASTROs IFNy	-128.4	-218.2 to -38.64	Yes	***	0.0001
H1 hASTROs IFNy vs. Mito234 hASTROs DMSO	97.77	8.011 to 187.5	Yes	*	0.0175
H1 hASTROs IFNy vs. Mito 234 hASTROs Monensin	133.5	43.04 to 224.0	Yes	****	<0.0001
H1 hASTROs IFNy vs. Mito 234 hASTROs IFNy	-114.3	-204.0 to -24.52	Yes	**	0.0014
H1 hASTROs IFNy vs. Hues8 hASTROs DMSO	98.06	8.297 to 187.8	Yes	*	0.0169
H1 hASTROs IFNy vs. Hues8 hASTROs Monensin	122.6	32.88 to 212.4	Yes	***	0.0003
H1 hASTROs IFNy vs. Hues8 hASTROs IFNy	2.336	-87.43 to 92.10	No	ns	>0.9999
H1 hASTROs IFNy vs. 1016A hASTROs DMSO	97.77	8.011 to 187.5	Yes	*	0.0175
H1 hASTROs IFNy vs. 1016A hASTROs Monensin	125.9	36.17 to 215.7	Yes	***	0.0002
H1 hASTROs IFNy vs. 1016A hASTROs IFNy	-168.5	-258.2 to -78.70	Yes	****	<0.0001

Primary HA DMSO vs. Primary HA Monensin	37	-74.42 to 148.4	No	ns	0.9995
Primary HA DMSO vs. Primary HA IFNy	-125.1	-234.1 to -16.17	Yes	**	0.0082
Primary HA DMSO vs. Mito80 hASTROs DMSO	-44.89	-139.3 to 49.48	No	ns	0.9705
Primary HA DMSO vs. Mito80 hASTROs Monensin	7.006	-87.36 to 101.4	No	ns	>0.9999
Primary HA DMSO vs. Mito80 hASTROs IFNy	-234.9	-329.2 to -140.5	Yes	****	<0.0001
Primary HA DMSO vs. Mito234 hASTROs DMSO	-8.696	-103.1 to 85.67	No	ns	>0.9999
Primary HA DMSO vs. Mito 234 hASTROs Monensin	27.05	-68.00 to 122.1	No	ns	>0.9999
Primary HA DMSO vs. Mito 234 hASTROs IFNy	-220.8	-315.1 to -126.4	Yes	****	<0.0001
Primary HA DMSO vs. Hues8 hASTROs DMSO	-8.41	-102.8 to 85.96	No	ns	>0.9999
Primary HA DMSO vs. Hues8 hASTROs Monensin	16.17	-78.20 to 110.5	No	ns	>0.9999
Primary HA DMSO vs. Hues8 hASTROs IFNy	-104.1	-198.5 to -9.765	Yes	*	0.0147
Primary HA DMSO vs. 1016A hASTROs DMSO	-8.696	-103.1 to 85.67	No	ns	>0.9999
Primary HA DMSO vs. 1016A hASTROs Monensin	19.47	-74.90 to 113.8	No	ns	>0.9999
Primary HA DMSO vs. 1016A hASTROs IFNy	-274.9	-369.3 to -180.6	Yes	****	<0.0001
Primary HA Monensin vs. Primary HA IFNy	-162.1	-273.5 to -50.71	Yes	****	<0.0001
Primary HA Monensin vs. Mito80 hASTROs DMSO	-81.89	-179.1 to 15.30	No	ns	0.2249
Primary HA Monensin vs. Mito80 hASTROs Monensin	-29.99	-127.2 to 67.19	No	ns	0.9998
Primary HA Monensin vs. Mito80 hASTROs IFNy	-271.9	-369.1 to -174.7	Yes	****	<0.0001
Primary HA Monensin vs. Mito234 hASTROs DMSO	-45.69	-142.9 to 51.49	No	ns	0.9736
Primary HA Monensin vs. Mito 234 hASTROs Monensin	-9.947	-107.8 to 87.90	No	ns	>0.9999
Primary HA Monensin vs. Mito 234 hASTROs IFNy	-257.8	-354.9 to -160.6	Yes	****	<0.0001
Primary HA Monensin vs. Hues8 hASTROs DMSO	-45.41	-142.6 to 51.78	No	ns	0.9752
Primary HA Monensin vs. Hues8 hASTROs Monensin	-20.83	-118.0 to 76.36	No	ns	>0.9999
Primary HA Monensin vs. Hues8 hASTROs IFNy	-141.1	-238.3 to -43.95	Yes	****	<0.0001
Primary HA Monensin vs. 1016A hASTROs DMSO	-45.69	-142.9 to 51.49	No	ns	0.9736
Primary HA Monensin vs. 1016A hASTROs Monensin	-17.53	-114.7 to 79.65	No	ns	>0.9999

Primary HA Monensin vs. 1016A hASTROs IFNy	-311.9	-409.1 to -214.7	Yes	****	<0.0001
Primary HA IFNy vs. Mito80 hASTROs DMSO	80.24	-14.13 to 174.6	No	ns	0.2113
Primary HA IFNy vs. Mito80 hASTROs Monensin	132.1	37.77 to 226.5	Yes	***	0.0002
Primary HA IFNy vs. Mito80 hASTROs IFNy	-109.7	-204.1 to -15.37	Yes	**	0.0067
Primary HA IFNy vs. Mito234 hASTROs DMSO	116.4	22.07 to 210.8	Yes	**	0.0025
Primary HA IFNy vs. Mito 234 hASTROs Monensin	152.2	57.13 to 247.2	Yes	****	<0.0001
Primary HA IFNy vs. Mito 234 hASTROs IFNy	-95.62	-190.0 to -1.253	Yes	*	0.0431
Primary HA IFNy vs. Hues8 hASTROs DMSO	116.7	22.35 to 211.1	Yes	**	0.0024
Primary HA IFNy vs. Hues8 hASTROs Monensin	141.3	46.93 to 235.7	Yes	****	<0.0001
Primary HA IFNy vs. Hues8 hASTROs IFNy	21	-73.37 to 115.4	No	ns	>0.9999
Primary HA IFNy vs. 1016A hASTROs DMSO	116.4	22.07 to 210.8	Yes	**	0.0025
Primary HA IFNy vs. 1016A hASTROs Monensin	144.6	50.23 to 239.0	Yes	****	<0.0001
Primary HA IFNy vs. 1016A hASTROs IFNy	-149.8	-244.2 to -55.43	Yes	****	<0.0001
Mito80 hASTROs DMSO vs. Mito80 hASTROs Monensin	51.9	-25.15 to 128.9	No	ns	0.6327
Mito80 hASTROs DMSO vs. Mito80 hASTROs IFNy	-190	-267.0 to -112.9	Yes	****	<0.0001
Mito80 hASTROs DMSO vs. Mito234 hASTROs DMSO	36.2	-40.85 to 113.2	No	ns	0.9739
Mito80 hASTROs DMSO vs. Mito 234 hASTROs Monensin	71.94	-5.942 to 149.8	No	ns	0.1099
Mito80 hASTROs DMSO vs. Mito 234 hASTROs IFNy	-175.9	-252.9 to -98.81	Yes	****	<0.0001
Mito80 hASTROs DMSO vs. Hues8 hASTROs DMSO	36.48	-40.57 to 113.5	No	ns	0.9718
Mito80 hASTROs DMSO vs. Hues8 hASTROs Monensin	61.06	-15.99 to 138.1	No	ns	0.3268
Mito80 hASTROs DMSO vs. Hues8 hASTROs IFNy	-59.24	-136.3 to 17.81	No	ns	0.3825
Mito80 hASTROs DMSO vs. 1016A hASTROs DMSO	36.2	-40.85 to 113.2	No	ns	0.9739
Mito80 hASTROs DMSO vs. 1016A hASTROs Monensin	64.36	-12.69 to 141.4	No	ns	0.2383
Mito80 hASTROs DMSO vs. 1016A hASTROs IFNy	-230	-307.1 to -153.0	Yes	****	<0.0001
Mito80 hASTROs Monensin vs. Mito80 hASTROs IFNy	-241.9	-318.9 to -164.8	Yes	****	<0.0001

Mito80 hASTROs Monensin vs. Mito234 hASTROs DMSO	-15.7	-92.75 to 61.35	No	ns	>0.9999
Mito80 hASTROs Monensin vs. Mito 234 hASTROs Monensin	20.04	-57.84 to 97.93	No	ns	>0.9999
Mito80 hASTROs Monensin vs. Mito 234 hASTROs IFNy	-227.8	-304.8 to -150.7	Yes	****	<0.0001
Mito80 hASTROs Monensin vs. Hues8 hASTROs DMSO	-15.42	-92.47 to 61.64	No	ns	>0.9999
Mito80 hASTROs Monensin vs. Hues8 hASTROs Monensin	9.165	-67.89 to 86.22	No	ns	>0.9999
Mito80 hASTROs Monensin vs. Hues8 hASTROs IFNy	-111.1	-188.2 to -34.09	Yes	****	<0.0001
Mito80 hASTROs Monensin vs. 1016A hASTROs DMSO	-15.7	-92.75 to 61.35	No	ns	>0.9999
Mito80 hASTROs Monensin vs. 1016A hASTROs Monensin	12.46	-64.59 to 89.51	No	ns	>0.9999
Mito80 hASTROs Monensin vs. 1016A hASTROs IFNy	-281.9	-359.0 to -204.9	Yes	****	<0.0001
Mito80 hASTROs IFNy vs. Mito234 hASTROs DMSO	226.2	149.1 to 303.2	Yes	****	<0.0001
Mito80 hASTROs IFNy vs. Mito 234 hASTROs Monensin	261.9	184.0 to 339.8	Yes	****	<0.0001
Mito80 hASTROs IFNy vs. Mito 234 hASTROs IFNy	14.12	-62.93 to 91.17	No	ns	>0.9999
Mito80 hASTROs IFNy vs. Hues8 hASTROs DMSO	226.5	149.4 to 303.5	Yes	****	<0.0001
Mito80 hASTROs IFNy vs. Hues8 hASTROs Monensin	251	174.0 to 328.1	Yes	****	<0.0001
Mito80 hASTROs IFNy vs. Hues8 hASTROs IFNy	130.7	53.69 to 207.8	Yes	****	<0.0001
Mito80 hASTROs IFNy vs. 1016A hASTROs DMSO	226.2	149.1 to 303.2	Yes	****	<0.0001
Mito80 hASTROs IFNy vs. 1016A hASTROs Monensin	254.3	177.3 to 331.4	Yes	****	<0.0001
Mito80 hASTROs IFNy vs. 1016A hASTROs IFNy	-40.06	-117.1 to 36.99	No	ns	0.9346
Mito234 hASTROs DMSO vs. Mito 234 hASTROs Monensin	35.75	-42.14 to 113.6	No	ns	0.9792
Mito234 hASTROs DMSO vs. Mito 234 hASTROs IFNy	-212.1	-289.1 to -135.0	Yes	****	<0.0001
Mito234 hASTROs DMSO vs. Hues8 hASTROs DMSO	0.2857	-76.77 to 77.34	No	ns	>0.9999
Mito234 hASTROs DMSO vs. Hues8 hASTROs Monensin	24.87	-52.18 to 101.9	No	ns	0.9997
Mito234 hASTROs DMSO vs. Hues8	-95.44	-172.5 to -18.39	Yes	**	0.0023

hASTROs IFNy					
Mito234 hASTROs DMSO vs. 1016A hASTROs DMSO	-6.668E-06	-77.05 to 77.05	No	ns	>0.9999
Mito234 hASTROs DMSO vs. 1016A hASTROs Monensin	28.16	-48.89 to 105.2	No	ns	0.9983
Mito234 hASTROs DMSO vs. 1016A hASTROs IFNy	-266.2	-343.3 to -189.2	Yes	****	<0.0001
Mito 234 hASTROs Monensin vs. Mito 234 hASTROs IFNy	-247.8	-325.7 to -169.9	Yes	****	<0.0001
Mito 234 hASTROs Monensin vs. Hues8 hASTROs DMSO	-35.46	-113.3 to 42.42	No	ns	0.9808
Mito 234 hASTROs Monensin vs. Hues8 hASTROs Monensin	-10.88	-88.76 to 67.00	No	ns	>0.9999
Mito 234 hASTROs Monensin vs. Hues8 hASTROs IFNy	-131.2	-209.1 to -53.30	Yes	****	<0.0001
Mito 234 hASTROs Monensin vs. 1016A hASTROs DMSO	-35.75	-113.6 to 42.14	No	ns	0.9792
Mito 234 hASTROs Monensin vs. 1016A hASTROs Monensin	-7.584	-85.47 to 70.30	No	ns	>0.9999
Mito 234 hASTROs Monensin vs. 1016A hASTROs IFNy	-302	-379.9 to -224.1	Yes	****	<0.0001
Mito 234 hASTROs IFNy vs. Hues8 hASTROs DMSO	212.3	135.3 to 289.4	Yes	****	<0.0001
Mito 234 hASTROs IFNy vs. Hues8 hASTROs Monensin	236.9	159.9 to 314.0	Yes	****	<0.0001
Mito 234 hASTROs IFNy vs. Hues8 hASTROs IFNy	116.6	39.57 to 193.7	Yes	****	<0.0001
Mito 234 hASTROs IFNy vs. 1016A hASTROs DMSO	212.1	135.0 to 289.1	Yes	****	<0.0001
Mito 234 hASTROs IFNy vs. 1016A hASTROs Monensin	240.2	163.2 to 317.3	Yes	****	<0.0001
Mito 234 hASTROs IFNy vs. 1016A hASTROs IFNy	-54.17	-131.2 to 22.88	No	ns	0.5536
Hues8 hASTROs DMSO vs. Hues8 hASTROs Monensin	24.58	-52.47 to 101.6	No	ns	0.9997
Hues8 hASTROs DMSO vs. Hues8 hASTROs IFNy	-95.72	-172.8 to -18.67	Yes	**	0.0022
Hues8 hASTROs DMSO vs. 1016A hASTROs DMSO	-0.2857	-77.34 to 76.77	No	ns	>0.9999
Hues8 hASTROs DMSO vs. 1016A hASTROs Monensin	27.88	-49.17 to 104.9	No	ns	0.9985
Hues8 hASTROs DMSO vs. 1016A hASTROs IFNy	-266.5	-343.6 to -189.5	Yes	****	<0.0001
Hues8 hASTROs Monensin vs. Hues8 hASTROs IFNy	-120.3	-197.4 to -43.25	Yes	****	<0.0001

Hues8 hASTROs Monensin vs. 1016A hASTROs DMSO	-24.87	-101.9 to 52.18	No	ns	0.9997
Hues8 hASTROs Monensin vs. 1016A hASTROs Monensin	3.295	-73.76 to 80.35	No	ns	>0.9999
Hues8 hASTROs Monensin vs. 1016A hASTROs IFNy	-291.1	-368.1 to -214.0	Yes	****	<0.0001
Hues8 hASTROs IFNy vs. 1016A hASTROs DMSO	95.44	18.39 to 172.5	Yes	**	0.0023
Hues8 hASTROs IFNy vs. 1016A hASTROs Monensin	123.6	46.55 to 200.6	Yes	****	<0.0001
Hues8 hASTROs IFNy vs. 1016A hASTROs IFNy	-170.8	-247.8 to -93.74	Yes	****	<0.0001
1016A hASTROs DMSO vs. 1016A hASTROs Monensin	28.16	-48.89 to 105.2	No	ns	0.9983
1016A hASTROs DMSO vs. 1016A hASTROs IFNy	-266.2	-343.3 to -189.2	Yes	****	<0.0001
1016A hASTROs Monensin vs. 1016A hASTROs IFNy	-294.4	-371.4 to -217.3	Yes	****	<0.0001

Table S2
Validation of 24 selected compounds using 1016A-hASTRO at 4 different concentrations

Compound	Concentration	% Secretion of C4 (DMSO 100%)			Average	Validated
Belinostat (PXD101)	1	95.2169815	123.5234765	104.6243127	107.7882569	Yes
	0.3	91.89608455	92.76030951	96.30264011	93.65301139	
	0.1	68.23005359	79.14196183	78.62576541	75.33259361	
	0.03	63.54194938	71.65700094	77.27826728	70.8257392	
Ibrutinib (PCI-32765)	1	83.56999764	98.02156495	91.96776864	91.18644374	No
	0.3	81.99842407	93.33271476	96.40280996	90.57798293	
	0.1	92.99533882	98.23330343	95.8977659	95.70880272	
	0.03	98.07704349	104.0754248	101.1784421	101.1103035	
GSK690693	1	58.75426735	66.95471968	69.14141915	64.95013539	Yes
	0.3	64.10548946	66.86248909	73.36242093	68.11013316	
	0.1	70.3177016	74.44880503	82.66515572	75.81055412	
	0.03	76.90184931	79.57479707	83.8365375	80.10439463	
Varespladib (LY315920)	1	87.8964463	87.22142366	88.85591699	87.99126232	Yes
	0.3	90.39282702	86.02299073	87.1774448	87.86442085	
	0.1	98.63932571	86.35215792	94.38084983	93.12411115	
	0.03	90.98801493	103.1711957	109.8685567	101.3425891	
AZD7762	1	428.0135222	353.0607578	246.7650333	342.6131044	Yes
	0.3	101.4098103	75.32060969	83.32667624	86.68569873	
	0.1	78.73642004	73.97142634	81.17640571	77.96141736	
	0.03	76.25622747	76.81839061	82.44848825	78.50770211	
GW9662	1	74.61052695	73.82237604	75.08148865	74.50479721	Yes
	0.3	74.16194372	77.083787	76.83362874	76.02645315	
	0.1	88.45101493	85.29311444	84.12572283	85.9566174	
	0.03	94.60764394	100.3253313	91.75010343	95.56102622	
LY2228820	1	83.46272218	94.27244298	89.66285358	89.13267291	Yes
	0.3	82.76632331	74.68972832	80.21547746	79.22384303	
	0.1	70.47357593	73.95570824	77.07523622	73.83484013	
	0.03	72.00591028	76.2146077	81.35085973	76.52379257	
IMD 0354	1	90.45184577	95.25979359	82.36408532	89.35857489	Yes
	0.3	60.34602274	56.28864941	55.84434866	57.49300694	
	0.1	58.28169705	54.34849913	46.69668068	53.10895895	
	0.03	103.8889257	106.66407	88.06620552	99.53973374	
I-BET151 (GSK1210151A)	1	78.91158792	76.97793766	77.95196323	77.94716294	Yes
	0.3	67.60396387	64.9129914	65.31898696	65.94531408	
	0.1	60.5288406	62.60796768	58.50765973	60.54815601	
	0.03	66.94705719	69.88867868	67.17754866	68.00442818	
Erastin	1	79.99510288	82.76262526	81.67271497	81.47681437	Yes
	0.3	88.72364361	87.17221559	87.24596288	87.71394069	
	0.1	96.86111558	91.61333981	86.92456436	91.79967325	
	0.03	105.9705779	108.0923435	99.41586504	104.4929288	
(+)-JQ1	1	75.19657934	79.16480919	78.85474141	77.73870998	Yes
	0.3	66.52840422	66.71362551	69.31264659	67.51822544	
	0.1	59.88210024	60.66952037	61.70045966	60.75069342	
	0.03	60.14089928	62.37701185	61.50552844	61.34114652	
ML161	1	84.010552	86.20036629	82.89221916	84.36771248	Yes
	0.3	89.17635192	90.82370106	84.80234635	88.26746644	
	0.1	95.31284703	96.67920796	85.08767872	92.35991123	
	0.03	106.6794618	105.862788	96.80206695	103.1147723	
Vildagliptin (LAF-237)	1	92.86335103	104.8711309	108.5931886	102.1092235	Yes
	0.3	89.03423407	86.74142787	92.87251633	89.54939276	
	0.1	81.45376409	86.50655818	88.58469245	85.5150049	
	0.03	81.57095851	86.94509178	94.96105718	87.82570249	
PTC-209	1	60.88401343	60.69267208	59.99760941	60.52476497	Yes
	0.3	96.41747525	88.08412925	93.69910968	92.73357139	
	0.1	94.17426218	93.74097315	89.76727858	92.56083797	
	0.03	108.7939802	111.7532315	103.5269119	108.0247079	
ABT-263 (Navitoclax)	1	87.41333962	105.870695	100.5848625	97.95629902	Yes
	0.3	90.73574511	94.02890454	99.24429766	94.66964911	
	0.1	85.13185048	88.16529121	94.17427785	89.15713985	

	0.03	91.35005206	86.08388999	98.49759471	91.97717892	
SGI-1027	1	80.92308677	93.16635012	88.31402846	87.46782178	Yes
	0.3	90.40017171	89.78852004	90.05043592	90.07970922	
	0.1	98.23272693	93.41645837	90.84699459	94.1653933	
	0.03	115.9928741	114.7690671	105.4690064	112.0769825	
Bosutinib (SKI-606)	1	85.1772622	91.47138095	83.5963562	86.74833312	Yes
	0.3	74.93109083	81.71920767	84.52823198	80.39284349	
	0.1	82.18221027	85.85486434	84.50255492	84.17987651	
	0.03	80.48689461	87.91206778	90.10366699	86.16754313	
Ruxolitinib (INCB018424)	1	80.96722201	87.05719514	80.45707879	82.82716531	Yes
	0.3	73.44676345	72.21225817	72.72301084	72.79401082	
	0.1	66.9308504	73.65611595	70.80592954	70.46429863	
	0.03	71.20937316	73.33368219	76.22871749	73.59059095	
MK-2206 2HCl	1	84.05291163	95.11900491	95.51319065	91.5617024	No
	0.3	85.69045185	95.06947341	101.5998704	94.11993188	
	0.1	91.93251475	96.13325985	98.8339452	95.63323993	
	0.03	97.42249037	93.7011677	105.6661796	98.9299459	
VX-745	1	99.50376677	113.935861	119.5180993	110.985909	No
	0.3	108.2053545	118.118848	122.2049908	116.1763978	
	0.1	116.1682534	116.1513317	121.9360275	118.0852042	
	0.03	113.3344424	124.2666808	127.3698014	121.6569749	
OTX-015	1	78.71617337	59.32152991	67.09027886	68.37599405	Yes
	0.3	61.80954442	60.77857342	70.84144142	64.47651975	
	0.1	62.58220759	63.3558413	79.86112016	68.59972302	
	0.03	62.87345176	71.4525039	102.6127065	78.97955406	
NMS-873	1	89.76377054	79.06161019	77.45860942	82.09466338	Yes
	0.3	81.18810678	78.023349	89.28950217	82.83365265	
	0.1	78.7908697	88.91999701	98.42465161	88.71183944	
	0.03	85.23053545	88.62753975	124.9402431	99.59943944	
Tofacitinib	1	72.67305317	57.30246064	62.0140359	63.99651657	Yes
	0.3	66.59902169	64.06034593	79.51121394	70.05686052	
	0.1	70.51200554	77.31229664	94.89409898	80.90613372	
	0.03	72.6500809	85.69045191	116.187631	91.50938794	
GSK1904529A	1	92.76478477	99.82876275	105.1572298	99.25025911	No
	0.3	99.26345563	102.9419078	112.368375	104.8579128	
	0.1	99.59804975	113.7800183	112.9462349	108.7747677	
	0.03	102.2262498	110.6111959	120.2550754	111.0308403	

Table S3
Validation of 24 selected compounds using Mito234-hASTRO at 4 different concentrations

Compound	Concentration	% Secretion of C4 (DMSO 100%)			Average	Validated
Belinostat (PXD101)	1	522.1910553	438.8527116	1027.093471	662.7124128	Nd
	0.3	220.7332291	213.4512381	229.339554	221.1746737	
	0.1	150.0758234	140.3596179	157.8343686	149.42327	
	0.03	110.3331529	130.8891834	121.5962393	120.9395252	
Ibrutinib (PCI-32765)	1	105.1186847	88.95934221	110.2589914	101.4456728	No
	0.3	102.515044	109.7486189	115.239956	109.167873	
	0.1	102.7596253	103.48677	106.9027155	104.3830369	
	0.03	93.14296846	114.9734637	127.6528421	111.9230914	
GSK690693	1	76.54799708	69.74280076	86.48464041	77.59181275	Yes
	0.3	71.9302617	68.16227494	79.51876399	73.20376688	
	0.1	70.46295559	75.9626701	86.479523	77.63504957	
	0.03	94.4542441	95.86453298	101.9788229	97.43253332	
Varespladib (LY315920)	1	91.53546215	91.37392898	109.6332578	97.51421632	No
	0.3	90.24238457	102.3872423	103.7369341	98.78885367	
	0.1	93.04504111	103.6451363	105.1567211	100.6156329	
	0.03	97.80439345	111.6016999	120.313305	109.9064661	
AZD7762	1	547.2598113	521.2717792	470.0326009	512.8547305	No
	0.3	151.9154489	134.9170286	152.5481281	146.4602019	
	0.1	125.9502618	100.8260868	115.814994	114.1971142	
	0.03	100.1755749	104.0994573	107.9015423	104.0588582	
GW9662	1	89.86008276	78.93393861	88.74271738	85.84557958	Yes
	0.3	101.1293804	84.69813549	91.57028791	92.46593459	
	0.1	95.69022361	100.1096194	114.1563943	103.3187458	
	0.03	98.22966834	117.0546776	113.8474167	109.7105875	
LY2228820	1	128.562789	105.1197898	136.0467296	123.2431028	Yes
	0.3	82.67275581	94.68925216	102.6229925	93.3283335	
	0.1	83.85350327	78.75526369	94.62622688	85.74499795	
	0.03	90.41853568	82.49478436	94.2054218	89.03958062	
IMD 0354	1	250.0607559	234.5815535	245.5594384	243.4005826	Nd
	0.3	174.3172734	140.2721332	143.6825871	152.7573312	
	0.1	108.9593955	109.0915244	115.0157861	111.0222353	
	0.03	125.5655989	116.9654265	125.0744685	122.5351646	
I-BET151 (GSK1210151A)	1	127.8497684	133.0424856	160.3189208	140.4037249	yes
	0.3	79.22563207	99.79042198	107.747432	95.58782868	
	0.1	80.24956741	74.10509807	87.48520755	80.61329101	
	0.03	80.8138032	77.81675235	84.7541729	81.12824281	
Erastin	1	96.02401712	94.65771067	108.2476605	99.64312944	No
	0.3	96.37618408	97.28715769	103.0833955	98.9155791	
	0.1	95.85593596	109.7189551	109.2061585	104.9270165	
	0.03	107.8174417	116.8215438	124.5642188	116.4010681	
(+)-JQ1	1	120.6489983	126.4673794	148.6104355	131.9089377	Yes
	0.3	88.03092198	95.3301949	102.4111162	95.25741103	
	0.1	87.33502963	79.6831507	87.63951876	84.8858997	
	0.03	76.80957793	75.83383152	84.17728915	78.94023287	
ML161	1	87.13661974	92.4217801	105.9787584	95.17905276	No
	0.3	97.38605458	93.93108413	110.0386576	100.4519321	
	0.1	101.1213005	98.89158988	114.2514397	104.7547767	
	0.03	110.4594469	117.8485286	128.6161987	118.9747248	
Vildagliptin (LAF-237)	1	108.7232541	97.36495482	138.9632822	115.0171637	No
	0.3	97.0112198	100.1777423	114.4804021	103.889788	
	0.1	96.51862174	98.12808887	106.1858107	100.2775071	
	0.03	97.70865936	99.30991792	105.7636268	100.9274014	
PTC-209	1	83.24641121	81.95252714	91.50233058	85.56708964	Yes
	0.3	95.3575607	103.9216548	106.3361869	101.8718008	
	0.1	104.0427914	103.6173317	114.1839674	107.2813635	
	0.03	104.1300541	116.172416	143.9418511	121.4147737	
ABT-263 (Navitoclax)	1	92.55864775	83.42050727	113.056786	96.34531366	No
	0.3	81.03278273	94.79330837	104.7237782	93.51662311	
	0.1	103.1948991	80.38901278	100.0953594	94.55975708	

	0.03	92.09185895	100.0299804	100.1230785	97.41497262	
SGI-1027	1	97.21099125	93.08548725	115.8763087	102.0575957	No
	0.3	101.235752	104.6297678	113.4187061	106.4280753	
	0.1	102.3881761	104.6352401	124.9114463	110.6449542	
	0.03	101.7448925	119.1731172	126.7881753	115.9020617	
Bosutinib (SKI-606)	1	111.8315705	101.823071	122.7940397	112.1495604	Yes
	0.3	87.37414817	90.79911392	104.5728193	94.24869381	
	0.1	86.69188691	78.29848837	90.88438271	85.291586	
	0.03	99.52521496	107.893675	100.5397675	102.6528858	
Ruxolitinib (INCB018424)	1	97.4694754	78.47101691	103.8354306	93.25864096	Yes
	0.3	79.08329487	76.61785331	87.91493605	81.20536141	
	0.1	73.82343602	73.04704072	76.71401306	74.52816327	
	0.03	78.1532461	90.65162264	92.32895076	87.0446065	
MK-2206 2HCl	1	122.952508	86.43238921	121.7941461	110.3930144	No
	0.3	110.5142731	95.42194722	104.9080292	103.6147499	
	0.1	121.576841	103.0396449	151.5953046	125.4039302	
	0.03	113.6403791	121.4060933	132.9991796	122.681884	
VX-745	1	101.5774408	99.67888112	104.1888008	101.8150409	No
	0.3	116.9595707	131.7087757	140.3384734	129.6689399	
	0.1	94.78617958	113.2004725	105.8339828	104.6068783	
	0.03	123.7051212	109.780596	137.4535557	123.6464243	
OTX-015	1	113.5198961	86.80908585	88.69971562	96.34289919	Yes
	0.3	85.24333486	76.74271794	86.07992777	82.68866019	
	0.1	74.35193751	71.93781406	88.22959859	78.17311672	
	0.03	68.79079574	76.50054963	100.8373975	82.0429143	
NMS-873	1	176.3793391	129.3243038	124.3433566	143.3489998	Yes
	0.3	85.15044137	99.90287703	94.82988454	93.29440098	
	0.1	94.05938609	99.19120564	102.1476623	98.46608467	
	0.03	98.64078096	99.93528587	115.3866277	104.6542315	
Tofacitinib	1	78.96799824	77.03337529	87.4769219	81.15943181	Yes
	0.3	70.06014262	85.85217873	99.92418397	85.2788351	
	0.1	84.15203722	106.1032416	107.5931145	99.28279778	
	0.03	92.58689517	106.7458166	115.3401935	104.8909684	
GSK1904529A	1	90.64523106	108.8199128	119.5046035	106.3232491	No
	0.3	105.5011303	105.9447315	112.306166	107.9173426	
	0.1	89.59743441	94.25893712	100.184306	94.68022585	
	0.03	87.80125587	105.1920121	115.8658765	102.9530482	

Table S4 Antibodies

Antibody	Host Animal	Company	Catalog number	Dilution	Application
CD44	Mouse	Cell Signaling	3750	1:400	Immunofluorescence
ALDH1L1	Rabbit	Abcam	Ab190298	1:250	Immunofluorescence
S100β	Mouse	Sigma	S2532	1:1000	Immunofluorescence
GFAP	Rabbit	Dako	M0761	1:400	Immunofluorescence
AQP4	RAbbit	Millipore	AB3594	1:100	Immunofluorescence
CX43	Rabbit	Sigma	C6219	1:500	Immunofluorescence
EAAT1 (SLC1A3)	Rabbit	Boster	PA2185	1:100	Immunofluorescence
P65	Mouse	Santa Cruz Biotechnology	SC-8008	1:500	Immunofluorescence
FITC Mouse Anti-Human CD44	Mouse IgG2b, κ	BD Pharmingen	555478	20 uL per test	FACS

PerCP-Cy 5.5 Mouse Anti-Human CD200	Mouse IgG1, κ	BD Pharmingen	562124	5 uL per test	FACS
FITC Mouse IgG2b κ Isotype Control	Mouse IgG2b, κ	BD Pharmingen	555742	20 uL per test	FACS
PerCP-Cy™5.5 Mouse IgG1 κ Isotype Control	Mouse IgG1, κ	BD Pharmingen	550795	5 uL per test	FACS
Polyclonal Antiserum to Human C4 Protein	Goat	Quidel	A305	1:1000	ELISA
C4c Complement (Conjugate)	Rabbit	Dako	F0169	1:3000	ELISA
Goat Anti-Rabbit IgG H&L (Alkaline Phosphatase)	Goat	Abcam	ab97048	1:5000	ELISA
Recombinant Anti-C4 antibody [EPR2990(2)]	Rabbit	Abcam	ab171577	1:1000	Western Blot
Recombinant Anti-Brd4 antibody [EPR5150(2)]	Rabbit	Abcam	128874	1:200	Western Blot
β-Actin	Mouse	Cell Signaling	8H10D10	1:20000	Western Blot
Histone H3 Antibody	Rabbit	Cell Signaling	9715	1:20000	Western Blot

Expression of human C4A	Forward: CCTGAGAAACTGCAGGAGACAT Reverse: GTGAGTGCCACAGTCTCATCAT Probe: FAM_CAGGACCCCTGTCCAGTGTTAGAC
Expression of human C4B	Forward: CCTGAGAAACTGCAGGAGACAT Reverse: GTGAGTGCCACAGTCTCATCAT Probe: FAM_CTATGTATCACTGGAGAGAGGTCCTGGAAC
Expression of GAPDH	ThermoFisher Scientific Catalog number: 402869
Copy number of human C4A (*)	Forward: CCTTTGTGTTGAAGGTCCTGAGTT Reverse: TCCTGTCTAACACTGGACAGGGGT Probe: VIC-CCAGGAGCAGGTAGGAGGCTCGC-MGB
Copy number of human C4B (*)	Forward: TGCAGGAGACATCTAACTGGCTTCT Reverse: CATGCTCCTATGTATCACTGGAAGA Probe: VIC-AGCACGGCTGACGGC-MGB
Copy number of human C4L (*)	Forward: TTGCTCGTTCTGCTCATTCCTT Reverse: GTTGAGGCTGGTCCCCAAGA

Table S5 Primers and TaqMan probes

	Probe	VIC-CTCCTCCAGTGGACATG-MGB
Copy number of human C4S (*)	Forward	TTGCTCGTTCTGCTCATTCCTT
	Reverse	GGCGCAGGCTGCTGTATT
	Probe	VIC-CTCCTCCAGTGGACATG-MGB
Copy number of human RPP30	Forward	GATTTGGACCTGCGAGCG
	Reverse	GCGGCTGTCTCCACAAGT
	Probe	FAM-CTGACCTGAAGGCTCT-MGB
Human C1S	Forward	TAGAGATGTGGTGCAGATAAC
	Reverse	AGGTTGACATTTCAGTTTGG
Human C2	Forward	GATCATGAAAATGGAACTGGG
	Reverse	ATCTGTCAGAAGGATGATGG
Human C3	Forward	GAACTGCCTTTGTCATCTTC
	Reverse	CAGACACGTACAAAGACTTC
Human C4	Forward	CAAACTCATTTTGGGGGAG
	Reverse	CAGTACAGGTTATCTCCAGTC
Human C5	Forward	GAGGAGTAGCAACCAAATTC
	Reverse	CAGGTGGATTTTCTGAAGAG
Human GAPDH	Forward	CTCTGCTCCTCCTGTTCGAC
	Reverse	GCGCCCAATACGACCAAATC

All sequences are provided in the 5' to 3' orientation. Assays identified with an asterisk (*) were based on Wu et al. doi:10.1021/ac202028g (2011).

SUPPLEMENTARY EXPERIMENTAL PROCEDURES

Human pluripotent stem cell lines

All experiments with the human ESC lines were reviewed and approved by the Harvard Embryonic Stem Cell Oversight Committee. The use of the iPSC lines by the Rubin lab was reviewed by the Harvard Committee on the Use of Human Subjects (the Harvard IRB) and determined not to constitute human subjects' research. The Mito234 and the Mito80 line from a schizophrenic patient was obtained from Bruce M. Cohen, McLean Hospital. H1 C4 KO cells were generated in Lindy Barrett's laboratory (Harvard University and the Broad Institute's Stanley Center for Psychiatric Research).

Human pluripotent stem cell cultures

iPSCs (1016A, Mito234 and Mito80) and ESCs (HUES8 and H1 C4 KO and WT) were cultured in StemFlex medium (ThermoFisher A3349401). When pluripotent stem cells reached 80-85% confluency, colonies were dissociated using 0.5 mM EDTA in calcium/magnesium-free PBS at room temperature and passaged on Matrigel (Corning 354234) coated on 10 or 15-cm^2 tissue culture dishes (Corning). When the H1 lines reached 90% confluency, cells were dissociated using Accutase (Innovative Cell Technologies) for 5 minutes of incubation at room temperature. All human pluripotent stem cells used were maintained below 15 passages and confirmed to be karyotypically normal and mycoplasma negative.

Stem cell adaptation and astrocyte differentiation in spinner flasks

Pluripotent stem cells were single-cell dissociated using Accutase (Innovative Cell Technologies), as previously described in (Rigamonti et al., 2016). Briefly, cells were seeded into a 125 mL spinner flask in 100 mL of mTeSR medium supplemented with 10 μM ROCK inhibitor Y-27632 (STEMCELL) at a concentration of $1x10^6$ cells/mL. The spinner flask was placed on a nine-position stir plate (Dura-Mag) at a speed of 55 RPM in a 37°C incubator with 5% CO_2. Under these conditions, cells spontaneously aggregate, forming pluripotent spheres. Medium was changed by taking the flask off the stir plate and allowing the cells to settle to the flask's bottom. We adopted a modified protocol as previously described (Emdad et al., 2012). At day 1 of differentiation, the medium was changed to KSR (15% KSR (Life Technologies), KO DMEM (Gibco), 1% Glutamax (Gibco), 1% non-essential amino acids NEAA (Millipore), 1% penicillin-

streptomycin (Gibco), and 0.1% 2-mercaptoethanol 1,000X liquid (Gibco)) with activin/TGF-β inhibitor SB431542 (R&D Systems) and Dorsomorphin (Stemgent) to a final concentration of 10 μM and 1 μM respectively. The medium was changed every day for the first 5 days. From day 6 to day 12, the medium was changed every 2 days with NB media (Neurobasal, Gibco), 2X N2 supplement 100X (Gibco), 1% Glutamax (Gibco), 1% NEAA (Gibco), 1% penicillin-streptomycin (Gibco) supplemented with Dorsomorphin, and different cytokines as specified. On day 6 and day 8, FGF2 and EGF (10 ng/mL) were added to the media. On day 10 and 12, FGF2, EGF, and CTNF (Miltenyi Biotec and R&D Systems) at a final concentration of 20 ng/mL concentration were added. On day 14, NB 2X N2 medium containing CTNF and FGF at a final concentration of 20 ng/mL was added. From day 16 onward, the medium was changed every 2 days (NB 2x N2 CTNF 20 ng/mL). For details about sphere dissociation, astrocytes culture and cryopreservation see Supplementary experimental procedures.

Sphere dissociation, astrocyte culture, and cryopreservation

On day 30, spheres were dissociated using 0.25% trypsin (Gibco 25200056) and plated on overnight Poly-L-Lysine (PLL) (MP BIOMEDICALS 02194544) coated plates. First, spheres were collected in a 15 mL tube and allowed to settle. The medium was removed, and the spheres were washed with 1X PBS. After the spheres settled down, the PBS was removed. Double the volume of 0.25% trypsin was added to the spheres, and the tube was incubated in a water bath at 37°C for 5-10 minutes. Spheres were shaken periodically until the suspension looked cloudy. A volume of FBS equal to the sphere volume of FBS was added to quench the trypsin. Cells were spun for 3 minutes at 300g. After removing the supernatant, 3 mL of dissociation buffer (1x PBS, 5% FBS,

25mM Glucose, and 5mM MgCl2) was added to the tube and spheres were mechanically dissociated using a 5 mL pipette. This operation was repeated until the spheres were completely dissociated. Single cells were filtered using a 40 μM filter and centrifuged at 300g for 3 minutes. Cells were resuspended and plated at the desired concentration on Poly-L-Lysine coated plates in complete Astrocytes Medium (AM, ScienCell Research Labs #1801) with FBS, Astrocyte Growth Supplement, and Penicillin/Streptomycin Solution (ScienCell Research Labs #0010, #1852, #0503), or cryopreserved in FBS with 10% DMSO.

Bright-field images and immunofluorescence

Astrocytes were plated on PLL coated 6 or 96 well plates at a density of $5X10^5$ cells and $3X10^4$ cells per well, respectively. The next day cells were fixed using 4% PFA for 15 minutes and washed with PBS three times. The cells were blocked in 10% horse serum, 0.01% Triton X-100 in PBS (for CD44 staining only) or 5% horse serum, 0.3% PBS Triton X-100, for 1 hour at room temperature. Primary antibodies were diluted as specified in Supplementary Table 4 in 5% horse serum at 4°C overnight, followed by washes in PBS and incubation with secondary antibodies (diluted 1:1000) and Hoechst (1:5000) for 1 hour at room temperature. The fluorescently conjugated antibodies used were goat anti-mouse IgG Alexa Fluor 488 (Life Technologies A11001) and goat anti-rabbit IgG Alexa Fluor 546 (Life Technologies A11010). Bright-field and immunofluorescence images were acquired using an inverted Eclipse Ti microscope (Nikon) and an ImageXpress Micro Confocal (Molecular Devices), respectively. All images were processed with Adobe Photoshop software. P65 staining and CD44

positive cells were quantified using Columbus Image Data Storage and Analysis System (PerkinElmer).

Flow Cytometry Analysis

Freshly dissociated or frozen astrocytes (passage 0) were cultured as previously described until they reached 80% confluency. Cells were detached using Trypsin-EDTA solution (Sigma, T3924). $1x10^6$ cells were stained following the manufacturer's instruction for cell surface antigens using directly conjugated antibodies: FITC CD44, (555478), CD200 PerCP-Cy5.5 (562124) or isotype controls FITC Mouse igG2B k (555742) and PerCP-Cy5.5 IgG1 k (550795). All antibodies were purchased from BD Pharmingen. Hoechst (1:5000) was used as a viability marker. Samples were processed on the LSRII flow cytometer (BD Biosciences, San Diego, CA), and data were analyzed with FlowJo software (Tree Star, Ashland, OR USA). Antibody dilutions are listed in Supplementary Table 4.

Phagocytosis Assay

Primary hASTROs and stem-cell derived astrocytes were plated at a density of $2X10^5$ cells per 24 well plate. The next day different concentrations of pHrodo Green Zymosan A BioParticles Conjugates (1, 5 and 10 μg) (P35365 Invitrogen) were resuspended in media and incubated with cells. After 12 hours cells were harvested as previously described, washed with PBS once and analyzed by flow cytometry. The percentage of GFP positive cells was analyzed using FlowJo.

Astrocytes treatment

Astrocytes were treated for 48 hours if not otherwise specified. IFNγ was used at a final concentration of 250 ng/mL, Monensin was used at 1 μM and Polyinosinic:polycytidylic acid (poly(I:C) at 10 μg/mL.

ScRNA-sequencing

For scRNA-sequencing experiments, cells were harvested and run through the 10X Chromium Single Cell 3' Reagents V3 system to isolate individual cells into droplets per the vendor's instructions (10X Genomics; San Francisco, CA). Samples were then sequenced on a NovaSeq 6000 system (Illumina) using a S2 flow cell at 2 x 100bp. Raw sequence data was demultiplexed and aligned following the standard Drop-Seq protocol (Macosko et al., 2015). Human experiments were aligned to the GRCh38 reference and Ensembl v89 gene models. Sequencing reads were then filtered to reads that mapped at high quality (MQ>=10) to the human genome.

Matrices were built from 10X Chromium Single Cell 3' Reagents V3 as described above. Any barcode with less than 200 genes and combined UMI matrices were used for downstream analysis using Seurat (v4.0.2) (Stuart et al., 2019). After that, barcodes were further filtered by the number of genes detected 500<nFeature_RNA<95000 and percent of mitochondrial and ribosomal genes to reduce the number of dying cells/debris: percent.mito<10. The matrix was then processed via the Seurat pipeline by using SCTransform on a merged object running the PreSCTIntegration() function according to the sctransform integration pipeline (Hafemeister and Satija, 2019). After quality filtering, barcodes were used to compute UMAP projections using numbers of Principal Components based on ElbowPlot analysis. UMAP projection was used to determine minimum number of clusters obtained at resolution=0.2 (FindClusters) as

described previously (Limone et al., 2021). Correlation analysis between and within lines was generated by measuring the average expression of all genes shared across cell line replicates. The unsupervised clustering was performed by integrating published datasets using LIGER. First, datasets were downsampled to the smallest dataset, then normalized using SCTransform with default settings. Then, datasets were integrated running the default LIGER workflow. Dataset references: Adult astrocytes - M1 Brain atlas (Bakken et al., 2021); Fetal cortex (Polioudakis et al., 2019); iPSCs-ExN (Nehme et al., 2018); iPSCs derived cells (Barbar *et al.*, 2020; Leng *et al.*, 2021) and GW25 PFC - fetal brain atlas (Bhaduri et al., 2021).

ELISA

All washes were performed three times using 150 μl of PBS-T (Tween 0.05%). All incubations were performed at 37°C unless otherwise specified. Antibodies were incubated in a volume of 50 μl per well. 96-well plates (Thermo Scientific 439454) were coated (overnight at 4°C) with goat anti-human C4 antibody (Quidel A305) in PBS. The next day, the plates were washed and incubated with a blocking solution (1% BSA in PBS) for 1 hour. After eliminating the blocking solution, 85 μL of astrocyte supernatant was added to each well and incubated for 1 hour and 30 minutes. Following washes, the samples were incubated with a rabbit anti-human C4 (Dako F 0169) for one hour. Also following washes, the plates were incubated for 30 minutes with goat-anti-rabbit Alkaline Phosphatase (Abcam ab97048). In the last step following additional washes, the plates were incubated with 1M diethanolamine buffer, 0.5 mM $MgCl_2$, pH 9.8 containing Phosphatase substrate (Sigma S0942). The reaction was stopped with 3M NaOH and read at 405 nm using a Molecular Devices SpectraMax M5 Reader. After

removal of the supernatant, 96 well plates were fixed for 15 minutes with 4% PFA at room temperature and stained with Hoechst (1:5000) for 30 minutes. 6-9 fields per well were imaged using the Operetta (PerkinElmer) or ImageXpress Micro Confocal (Molecular Devices). Nuclei numbers were quantified using Columbus Image Data Storage and Analysis System (PerkinElmer) and used to normalize secretion absorbance data. Antibodies were diluted as specified in Supplementary Table 4.

Cytokine array

Astrocytes were plated in 6 well plates at a density of $5x10^5$ cells per well in complete AM media (ScienCell Research Labs). The next day, the medium was replaced with complete AM medium plus treatment; after 48 hours, the supernatant was collected and stored at -80°C. Proteome Profiler™ Human Cytokine Array (R&D Systems, #ARY005B) was used according to the manufacturer's guidelines. Proteome profiler intensity dot blots were quantified using Adobe Photoshop software.

C4 KO cell line generation

The XY human embryonic stem cell line H1 was commercially obtained from WiCell Research Institute. CRISPR-Cas9 based genome engineering experiments were carried out as previously described (Hazelbaker et al., 2017). In brief, to generate the C4 deletion line and wild-type control, 1.5 $x10^5$ H1 cells were transfected with 5pmol EnGen Cas9 NLS (New England BioLabs) plus 2.5pmol each of 5' and 3' gRNAs (Synthego) using the NEON system (Life Technologies). 5’ gRNA target sequence: ACGTTTGCCACATATACATA; 3’ gRNA target sequence: TATTGCCTGCACAGTTGATG. Transfected cells were then clonally isolated, followed

by deep sequencing and subcloning. PCR analysis and Sanger sequencing were used to confirm a 64.5kb deletion at the C4 locus. The wild-type control line went through targeting, clonal selection and subcloning but remained unedited at the C4 locus. SNP genotyping with the Infinium PsychArray (Illumina) was used to confirm an absence of chromosomal aberrations in C4 deletion and wild-type lines.

Ngn2 differentiation, ACM collection and treatment, synaptic isolation and C4 western blot

H1 C4 WT or C4 KO ESCs were dissociated with Accutase (Innovative Cell Technologies) and plated as single cells in Matrigel-coated 6 wells at a density of $1X10^6$ in complete StemFlex with 10 μM ROCK inhibitor Y-27632 (STEMCELL). The day after, the rtTA and TetON Ngn2 lentiviruses (purchased from ALSTEM) were added in fresh StemFlex media (1μl each per wells). After 24 hours, the medium was changed, and infected cells were allowed to recover and expand. Ngn2 differentiation was performed as described in (Zhang et al., 2013), with minor modifications. Briefly, ESC cells were plated on Matrigel-coated plates at a density of 3-5 $x10^6$ cells per 10 cm plates in mTesR with Rock inhibitor (10 μM). For the first two days, cells were fed with N2/DMEM/F12/NEAA (Invitrogen) containing human BDNF (10 ng/mL, Miltenyi Biotec), human NGF (10 ng/mL, R&D Systems). Doxycycline (2 μg/mL, Takara Bio to activate the TetON transgene). On day 3, medium was switched to B27/Glutamax NB media (Invitrogen) containing BDNF and NGF. On day 4, cells containing the transgene were selected by adding puromycin to the medium (1 μg/mL Thermo Fisher Scientific). On day 5, cells were replated on PO-laminin coated dishes in the presence of Ara-C (final concentration 2 μM). From day 5, B27/Glutamax medium was replaced every other day.

Cells were frozen on day 10 in CryStor CS10 ($25X10^6$ cells/mL) or differentiated until day 30 for experiments. Astrocyte-conditioned medium (ACM) was collected from 90% confluent astrocytes incubated for 48 hours with B27/Glutamax NB media. The supernatant was spun at 300g for 3 minutes, neuronal growth factors (BDNF and NGF) were added at a final concentration of 10 ng/mL and incubated with Ngn2 neurons for 24 hours. ACM was concentrated using 3K Amicon columns (according to the manufacture protocol) for loading on a Western Blot gel. For synaptosome purification, $30X10^6$ Ngn2 differentiated neurons were plated at day 10 on Poly-L-ornithine/Laminin coated plates. Medium was changed every 3 days. Neurons were treated with ACM for 24 hours. Synaptosomes were purified using SynPER (Thermo Fisher Scientific) following the manufacturer's datasheet. Synaptosomes were resuspended in PBS with 5% DMSO. Cells were lysed using RIPA buffer (Sigma Aldrich R0278) with protease inhibitors (Thermo Scientific 78426) and phosphatase inhibitors (78426). Whole-cell lysates concentrated, ACM or synaptosomes were loaded on a NuPAGE 4-12% Bis-Tris gel (Invitrogen) in equal amounts (50 μg) and transferred to polyvinylidene difluoride membrane using a transfer apparatus according to the manufacturer's protocols (Bio-Rad). After incubation with 5% milk in TBST (TBST (10 mM Tris, pH 8.0, 150 mM NaCl, 0.5% Tween 20) for 1 hour, the membrane was washed 3 times with TBST and incubated with antibodies against C4 in 3% TBST overnight at 4°C. Membranes were washed three times for 10 minutes and incubated with a 1:10000 dilution of horseradish peroxidase-conjugated anti-rabbit antibodies for 1 hour. Western blots were washed with TBST three times and developed with the SuperSignal West Dura Chemiluminescent Substrate (Thermo Scientific 34075).

Screen, hit selection, secondary screen and dose-response

96 well μ-clear black imaging plates (Greiner #655090) were coated with Poly-L-Lysine (MP Biomedicals #0215017610) at a final concentration of 15 μg/mL using the liquid handler BioTek EL406 (Agilent). Plates were incubated overnight at 37°C. The day after, plates were washed 3 times with PBS, and AM media was added to each well. Coating, washes, and media addition were performed using the BioTek EL406 liquid handler. 1016A-derived astrocytes were plated at a concentration of $3X10^4$ cells per well using the Multidrop™ Combi Reagent Dispenser (Thermo Scientific). The day after, the media was replaced with fresh media, and compounds were added at two different concentrations (1 and 0.3 μM) using the Thermo Scientific Matrix Hydra II 96-Channel Automated Liquid Handling System. The screen was performed in triplicate plates using the highly selective inhibitor Library (464 compounds) from Sellckchem. Two days after compound addition, the supernatant was used to perform ELISA (as previously described). Plates were stained with Hoechst using the Multidrop™ Combi Reagent Dispenser and quantified using the Operetta High-content imaging system from PerkinElmer. Nuclei were counted using the Columbus Image Data Storage and Analysis System (PerkinElmer). To exclude false positives due to cell toxicity, absorbance O.D. 405 was divided by nuclei number and normalized on DMSO control (100%). Compounds were ranked by the percentage decrease of C4. The top 24 compounds were selected for a secondary validation screen. The secondary screen was performed as previously described. Cherry-picked compounds from the stock library or freshly purchased compounds were tested at 4 concentrations (3, 1, 0.3, and 0.1 μM) in triplicates in 1016A-hASTRO. Compounds in the secondary screen were

considered to be validated when showing relatively minor toxicity (nuclei number greater or equal to 75% compared to DMSO control) and a C4 decrease greater than 10%. The same criteria were applied when testing compounds on Mito234-hASTROs. 12-point dose-responses (starting a 10 μM with 1 to three dilutions) were performed with selected compounds in stem-cells derived astrocytes. The concentration values (X) were converted into logarithmic scale and normalized. Nonlinear regression, variable slope (four parameters) was used to interpolate the data and calculate the IC_{50} using GraphPad.

Droplet digital PCR (ddPCR) of C4 structural elements

The copy number and structural variation of C4 genes were measured as previously described (Sekar et al., 2016). Genomic DNA was extracted using the Genomic DNA Extraction Kit from Qiagen following manufacturer's instruction. Each gDNA was digested with *AluI* at 37°C for 1 hour. The digested DNA was used to generate droplets containing gDNA, a specific primer-probe mix for (C4A and C4L or C4B and C4S), and a reference locus (RPP30). TaqMan probes are listed in Supplementary Table 5. The droplets were generated using a microfluidic droplet generator (Bio-Rad). The droplets containing this reaction mixture were subjected to PCR using the following cycling conditions: 95°C for 10 minutes, 40 cycles of 94°C for 30 seconds, and 60°C (for C4A and C4L) or 59°C (for C4B and C4S) for 1 minute, followed by 98°C for 10 minutes. After PCR, the fluorescence (both colors) in each droplet was read using a QX100 Droplet Reader (Bio-Rad). Data were analyzed using the QuantaSoft software (Bio-Rad), which estimates the absolute concentration of DNA templates by Poisson-correcting the fraction of droplets that are positive for each amplicon (C4 or RPP30).

qPCR and TaqMan probes (primers)

RNA was purified using the RNeasy Mini Kit (QIAGEN). cDNA was prepared with iSCRIPT (BioRad). All quantitative RT-PCR (qRT-PCR) reactions were performed in triplicate using the SYBER green PCR Master Mix (Applied Biosystems), and data were acquired on the QuantStudioTM 12K Flex Real-Time PCR System (Life Technologies). Ct values were calculated and normalized to the housekeeping gene, and the relative expression ratio was calculated using the Pfaffl method (Pfaffl, 2001). To detect C4A and C4B TaqMan probes and TaqMan Universal Master Mix II, no UNG was used following manufacture guidelines. TaqMan GAPDH control reagent was purchased from Thermo Fisher Scientific. Primers and TaqMan sequences are listed in Supplementary Table 5.

Chromatin purification and Western blot

Cells were cultured as previously described and treated with DMSO or JQ1 for 24 hours. Cells were collected using trypsin-EDTA solution, washed once with cold PBS, and fast-frozen. The chromatin-bound fraction and the cytoplasmic fraction were isolated using Thermo Scientific's Kit (78840) following the manufacturer's instruction. Equal amounts of proteins (5 μg) were loaded on a gel, as previously described. Antibody incubation was done overnight in 5% BSA in T-BST at 4°C with gentle agitation. Antibodies used are listed in Supplementary Table 4.

L1000 data generation

1016A-hASTROs and Mito234-hASTROs were plated at a density of 3000 cells/well in AM complete media in PLL coated 384 well plates. The day after, cells were treated

with 40 compounds at three different concentrations in triplicate with each cell line on a separate 384-well plate. Cells were lysed after 48 hours and were then subject to L1000 profiling as described in (Subramanian et al., 2017). Briefly, mRNA was captured using oligo-dT coated beads and reverse transcribed to cDNA. The cDNA was then PCR amplified using biotinylated, barcoded primers and gene-specific juxtaposed probe pairs resulting in gene-specific, barcoded, and biotinylated PCR amplicons. These amplicons were then hybridized to Luminex beads, stained with streptavidin R-phycoerythrin (SAPE) and detected on a FlexMAP 3D scanner, which for each bead reports the barcode, which determines gene identity, and the SAPE fluorescent intensity, which is indicative of transcript abundance.

L1000 data processing

L1000 data were processed into perturbagen-specific differential expression signatures as previously described (Subramanian et al., 2017). Briefly, raw fluorescent intensities (FI) were captured from the Luminex FlexMAP 3D scanner for each of the 978 L1000 landmark genes (Level 1 data). FI data were deconvoluted to extract the median FI (MFI) for the two genes being measured by each Luminex bead barcode (Level 2 data). MFI values were loess-normalized to the ten L1000 invariant gene sets within each well, and all wells on the same detection plate were then quantile normalized, resulting in each sample having the same empirical distribution (Level 3 data). Gene-wise robust z-scores were then computed for each sample, using all other samples on the same plate as the reference distribution (Level 4 data). Biological replicates were then collapsed using a weighted average, where each replicate was weighted by its average correlation

with the others (Level 5 data). The collection of Level 5 signatures is henceforth referred to as the C4-CMap dataset.

Query analysis

The C4-CMap signatures were converted into gene sets by extracting the top and bottom 50 most differentially expressed genes according to the Level 5 z-score. These gene sets were then queried into the CMap Touchstone (TS) database as described in (Subramanian et al., 2017). Briefly, two-sided weighted connectivity scores (WTCS) were computed for each C4-CMap gene set relative to each TS signature. WTCS values were then normalized within each Touchstone cell line / perturbagen type combination to yield normalized connectivity scores (NCS). Using the pre-computed reference NCS distributions for each TS signature, tau values were then computed as the fraction of reference NCS values more extreme than the observed NCS value for each C4-CMap gene set / TS signature combination. Cell-summarized tau ($tau_{summary}$) values were computed in a similar manner, using max-quantile aggregated NCS and reference NCS values as input.

Preferential connectivity analysis

C4-CMap signatures were identified as C4-reducing according to the corresponding compound's effect on C4 and lack of effect on cell fitness, using data from the C4 ELISA experiment. The criteria were: % C4 reduction ≥ 20 AND % nuclei ≥ 90, resulting in n=11 signatures. These signatures were then manually grouped according to the compounds' canonical mechanism of action (MoA), resulting in two groups. Group I contained exclusively bromodomain inhibitors and Group II contained compounds

whose targets include p97, AKT, and PLA. Contrastingly, we identified the C4-CMap signatures corresponding to un-interesting effects on C4 and/or cell fitness using the criteria of % C4 reduction < 10 OR % nuclei < 85, resulting in n=34 signatures. We then assessed the frequency with which each TS signature connected to the C4-CMap signatures in Groups I and II as well as to the un-interesting C4-CMap signatures, using a threshold of $tau_{summary} \geq 90$. C4 preferential connectors were those that frequently connected to the C4-reducing signatures and infrequently to the un-interesting signatures.

References

Bakken, T.E., Jorstad, N.L., Hu, Q., Lake, B.B., Tian,W., Kalmbach, B.E., Crow, M., Hodge, R.D., Krienen, F.M., Sorensen, S.A., et al. (2021). Comparative cellular analysis of motor cortex in human, marmoset and mouse. Nature 598, 111–119. https://doi.org/10.1038/s41586-021-03465-8.

Bhaduri, A., Sandoval-Espinosa, C., Otero-Garcia, M., Oh, I., Yin, R., Eze, U.C., Nowakowski, T.J., and Kriegstein, A.R. (2021). An atlas of cortical arealization identifies dynamic molecular signatures. Nature 598, 200–204. https://doi.org/10.1038/s41586-021-03910-8.

Hafemeister, C., and Satija, R. (2019). Normalization and variance stabilization of single-cell RNA-seq data using regularized negative binomial regression. Genome Biol. 20, 296. https://doi.org/10.1186/s13059-019-1874-1.

Hazelbaker, D.Z., Beccard, A., Bara, A.M., Dabkowski, N., Messana, A., Mazzucato, P., Lam, D., Manning, D., Eggan, K., and Barrett, L.E. (2017). A scaled framework for CRISPR editing of human pluripotent stem cells to study psychiatric disease. Stem Cell Rep. 9, 1315–1327. https://doi.org/10.1016/j.stemcr.2017.09.006.

Limone, F., Mordes, D.A., Couto, A., Pietilainen, O., Joseph, B.J., Burberry, A., Mitchell, J.M., Ghosh, S., Meyer, D., Therrien, M., et al. (2021). Single-nucleus sequencing reveals enriched expression of genetic risk factors sensitises Motor Neurons to degeneration in ALS. Preprint at bioRxiv. https://doi.org/10.1101/2021.07.12.452054.

Nehme, R., Zuccaro, E., Ghosh, S.D., Li, C., Sherwood, J.L., Pietilainen, O., Barrett, L.E., Limone, F., Worringer, K.A., Kommineni, S., et al. (2018). CombiningNGN2

programming with developmental patterning generates human excitatory neurons with NMDARmediated synaptic transmission. Cell Rep. 23, 2509–2523. https://doi.org/10.1016/j.celrep.2018.04.066.

Pfaffl, M.W. (2001). A new mathematical model for relative quantification in real-time RT-PCR. Nucleic Acids Res. 29, e45. https://doi.org/10.1093/nar/29.9.e45.

Polioudakis, D., de la Torre-Ubieta, L., Langerman, J., Elkins, A.G., Shi, X., Stein, J.L., Vuong, C.K., Nichterwitz, S., Gevorgian, M., Opland, C.K., et al. (2019). A single-cell transcriptomic atlas of human neocortical development during mid-gestation. Neuron 103, 785–801.e8. https://doi.org/10.1016/j.neuron.2019.06.011.

Stuart, T., Butler, A., Hoffman, P., Hafemeister, C., Papalexi, E., Mauck, W.M., 3rd, Hao, Y., Stoeckius, M., Smibert, P., and Satija, R. (2019). Comprehensive integration of single-cell data. Cell 177, 1888–1902.e21. https://doi.org/10.1016/j.cell.2019.05.031.

Zhang, Y., Pak, C., Han, Y., Ahlenius, H., Zhang, Z., Chanda, S., Marro, S., Patzke, C., Acuna, C., Covy, J., et al. (2013). Rapid single-step induction of functional neurons from human pluripotent stem cells. Neuron 78, 785–798. https://doi.org/10.1016/j.neuron. 2013.05.029.